

# Geochronology, geochemistry and zircon Hf-isotopes of the early Mesoproterozoic Yaopengzi dolerite in SW Yangtze block (Sichuan, SW China): implications for the Columbia supercontinent breakup

Tianguo Wang<sup>1</sup>, Chaowen Huang<sup>1</sup>, Gaofeng Du<sup>2\*</sup>, Yang Liu<sup>3</sup>, Jianfeng Xie<sup>4</sup>, and Huan Li<sup>1</sup>

<sup>1</sup>Key Laboratory of Metallogenetic Prediction of Nonferrous Metals and Geological Environment Monitoring, Ministry of Education, School of Geosciences and Info-Physics, CentralSouth University, Changsha 410083, China

<sup>2</sup>Department of Geochemical and Environmental Sciences, School of Earth and Space Sciences, University of Science and Technology of China, Hefei 230026, China

<sup>3</sup>Hunan Provincial Key Laboratory of Shale Gas Resource Utilization, Hunan University of Science and Technology, Xiangtan 411201, China

<sup>4</sup>Research Institute of Hunan Provincial Nonferrous Metals Geological Exploration Bureau, Hunan Provincial Nonferrous Metals Geological Exploration Bureau, Changsha 410015, China

**ABSTRACT:** Magmatism in the Huili area (SW margin of the Yangtze block) was active during the early Mesoproterozoic, and has important implications on the early tectonic evolution of the Yangtze block. We report new data in petrology, whole-rock geochemistry, zircon U-Pb and Hf isotopes for the Yaopengzi dolerite in the Huili area. LA-ICP-MS zircon U-Pb dating of the dolerite yielded an early Mesoproterozoic age of ca. 1515–1513 Ma, coeval with the Columbia supercontinent breakup. The dolerite belongs to the alkali basalt series, and is enriched in light rare earth elements (LREE) and large ion lithophile elements (LILE), resembling typical oceanic island basalt (OIB) in geochemistry. Zircons from the Yaopengzi dolerite yielded  $^{176}\text{Hf}/^{177}\text{Hf} = 0.28192\text{--}0.28203$  and  $\epsilon_{\text{Hf(t)}} = -0.3\text{ to }5.3$ . Our integrated study suggests that parental magma of the Yaopengzi dolerite may have originated from the enriched mantle, and was slightly contaminated by crustal materials during its evolution. Combining with regional tectonic background, the early Mesoproterozoic mafic magmatism at/around Yaopengzi may have formed in a mantle plume-related intracontinental rift setting. This reflects that the early Mesoproterozoic extension in the Yangtze block may have resulted from mantle plume activities led by the Columbia supercontinent breakup.

**Key words:** Yaopengzi dolerite, SW Yangtze block, Mesoproterozoic, zircon U-Pb and Hf isotopes, Columbia Supercontinent

Manuscript received November 24, 2017; Manuscript accepted December 7, 2018

## 1. INTRODUCTION

The Columbia supercontinent was likely assembled during ca. 2.1 to 1.8 Ga, and broken up during ca. 1.6 to 1.2 Ga (Rogers et al., 2002; Zhao et al., 2002), marked by widespread continental rifting, anorogenic magmatism and emplacement of mafic dyke swarms in most cratons, e.g., Congo-São Francisco, North China, Baltica, Laurentia, India and Australia (Meert and Santosh,

2017). The Yangtze block is one of the oldest geological terranes in China. In recent years, numerous Paleo-Mesoproterozoic magmatic rocks (ca. 2.1–1.6 Ga) have been recognized from the block. Much tectonothermal evidence related to the Columbia supercontinent assembly-breakup was reported inside/around the block (Zhang et al., 2006a, 2006b; Peng et al., 2012; Fan et al., 2013; Wang et al., 2014a; Zhang et al., 2016). These include the ultra-high temperature (UHT) granulite (ca. 2.1–1.8 Ga Hu et al., 2012; Lei et al., 2014) in the Sulu orogenic belt (NE margin of the Yangtze block) related to the extensive collisional-related orogeny during the supercontinent assembly, and the post-collisional extension-related anorogenic bimodal magmatism (ca. 1.8–1.6 Ga) in the SW Yangtze margin (Zhao et al., 2010; Wang et al., 2013a; Wang et al., 2014a; Yang, 2014).

The tectonic affinity of Mesoproterozoic magmatic rocks is

\*Corresponding author:

Gaofeng Du

Department of Geochemical and Environmental Sciences, School of Earth and Space Sciences, University of Science and Technology of China, No. 96, JinZhai Road, Baohe District, Hefei, Anhui 230026, China  
 Tel: +86-18607310708, E-mail: hbwhdgf2@ustc.edu.cn

important for understanding the role and location of the block in the Columbia supercontinent breakup. Nevertheless, Mesoproterozoic magmatism (ca. 1.6–1.2 Ga) for the subsequent supercontinent breakup is rarely reported in the Yangtze block, in contrast with the widespread post-orogenic/anorogenic magmatism in Precambrian terranes worldwide (Roy et al., 2002; Goldberg, 2010; Teixeira et al., 2012; Ernst et al., 2013; Silveira et al., 2014). The Yangtze block remains little known within Columbia Supercontinent breakup and requires additional investigations.

The mafic dyke intrusions play an important role on the study of supercontinent breakup (Wang et al., 2014). Recently, some Mesoproterozoic mafic dyke intrusions (ca. 1.6–1.2 Ga) have been recognized in the western margin of the Yangtze block, e.g., Zhuqing V-Ti-magnetite ore-bearing mafic intrusions (Fan et al., 2013), Jiaopingdu mafic intrusions and Yaopengzi mafic intrusions. V-Ti-magnetite ore-bearing mafic intrusions were found at Zhuqing, whose geochemical and Nd-isotopic evidence suggests that the parental magma may have originated from partial melting of relatively enriched mantle in an intracontinental rift setting (Fan et al., 2013). At Jiaopingdu-Yaopengzi, ore-barren dolerite-diorite dyke swarms are outcropped. Since the Zhuqing

V-Ti-magnetite ore-bearing layered intrusive rocks are cumulates and contain high Fe-Ti contents, the magma may have sourced from a highly-fractionated high-Ti magma that does not reflect the parental magma characteristics (Wager and Brown, 1968; Zhou et al., 2008; Fan et al., 2013). Therefore, we focused on the ore-barren dolerite at Yaopengzi, reported its zircon U-Pb ages and Hf isotopes and whole-rock geochemistry. We discussed the nature of the magma source and the possible tectonic setting to unravel the Mesoproterozoic tectonic evolution of the western margin of the Yangtze block, as well as its interrelationships with the Columbia supercontinent breakup.

## 2. BACKGROUND GEOLOGY

The western margin of the Yangtze block is situated among the Songpan-Ganzi orogenic belt (Fig. 1a), the Sanjiang orogenic belt and the Cathaysia block. The Yaopengzi area (in Huili County) is located in the central part of the western margin of the Yangtze block, and geologically comprises medium-low-grade metamorphosed volcanics-sediments of the Paleoproterozoic Hekou, Paleo-Mesoproterozoic Dongchuan and Mesoproterozoic Huili groups and Phanerozoic cover (Fig. 1b).

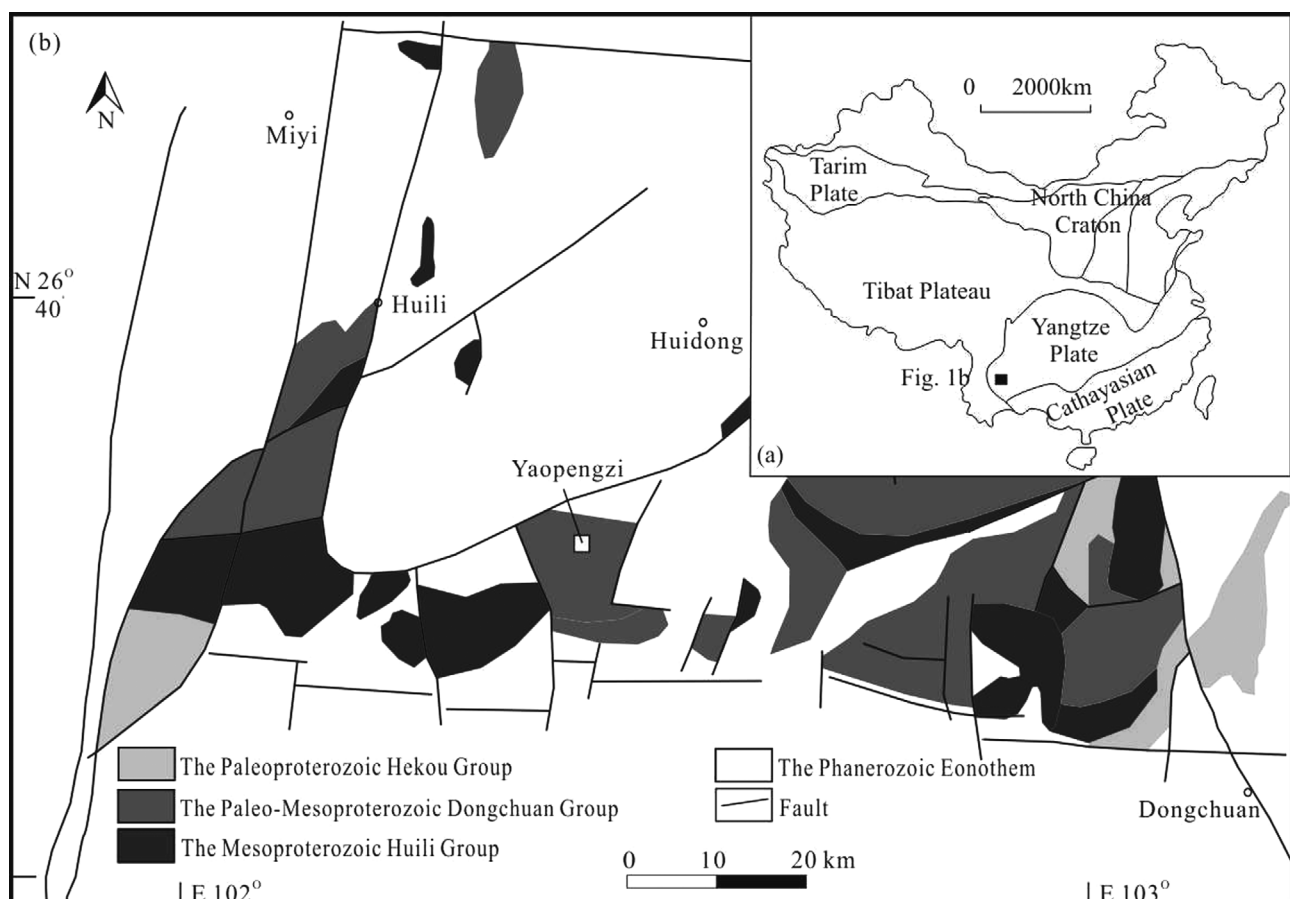


**Fig. 1.** (a) Geological sketch map of the Yangtze Block (modified from Zhao et al., 2010); (b) Sketch map of geology in the Huili-Dongchuan area (modified from Wu et al., 1990).

The Dongchuan Group is the most widespread, and contains (from oldest to the youngest) the Yinmin ( $Pt_2y$ ), Luoxue ( $Pt_2l$ ), Heishan ( $Pt_2h$ ), Qinglong ( $Pt_2q$ ) formations. The Yinmin Formation ( $Pt_2y$ ) is composed of purplish-grey banded sandy slate interbedded with muddy dolomite in the upper part, and purplish-grey sandy slate, black carbonaceous slate, volcanics and mafic volcanics (spillite) in the lower part. Breccias occur at the bottom of the sequence. The Luoxue Formation ( $Pt_2l$ ) is consisted of the bluish-grey/yellow dolomite, silicified dolomite, muddy-sandy dolomite and slate interbeds in the upper part, and white/grayish white dense dolomite in the lower part. One to two thin layers of yellowish-white muddy dolomite occur at the bottom of the sequence. The Heishan Formation ( $Pt_2h$ ) is consisted of black carbonaceous slate, sericite slate and silty slate. Interbeds (with well-developed slaty structure) of tuffaceous sandstone and slate occur in the middle part of the sequence. The Qinglong

Formation ( $Pt_1q$ ) is consisted of bluish-grey dolomite. Mafic rocks are widespread along the NNW faults, and are distributed mainly in the Yinmin–Sanfengkou–Tuobuka area (Dongchuan County, Yunnan Province) and the Jiaopingdu–Yaopengzi–Zhuqing area (Huili County, Sichuan Province). The mafic rocks (ca. 1.7–1.5 Ga) occur mainly as small dykes/sheeted dykes, and contain mainly gabbro, dolerite and diorite (Geng, 2012; Wang, 2013a; Wang, 2014a).

Eight samples were collected from the NW-trending dolerite dykes (2–10 m in width) at Yaopengzi, which intruded the Yinmin to Heishan formations along faults (Fig. 2a). The mafic rock samples are fresh, massive and light grayish-green, and show doleritic texture under the microscope (Fig. 2b). The dolerite contains mainly pyroxene (30%) and euhedral to subhedral plagioclase (60%), and minor amphibole (4%) and magnetite (Fig. 2c).

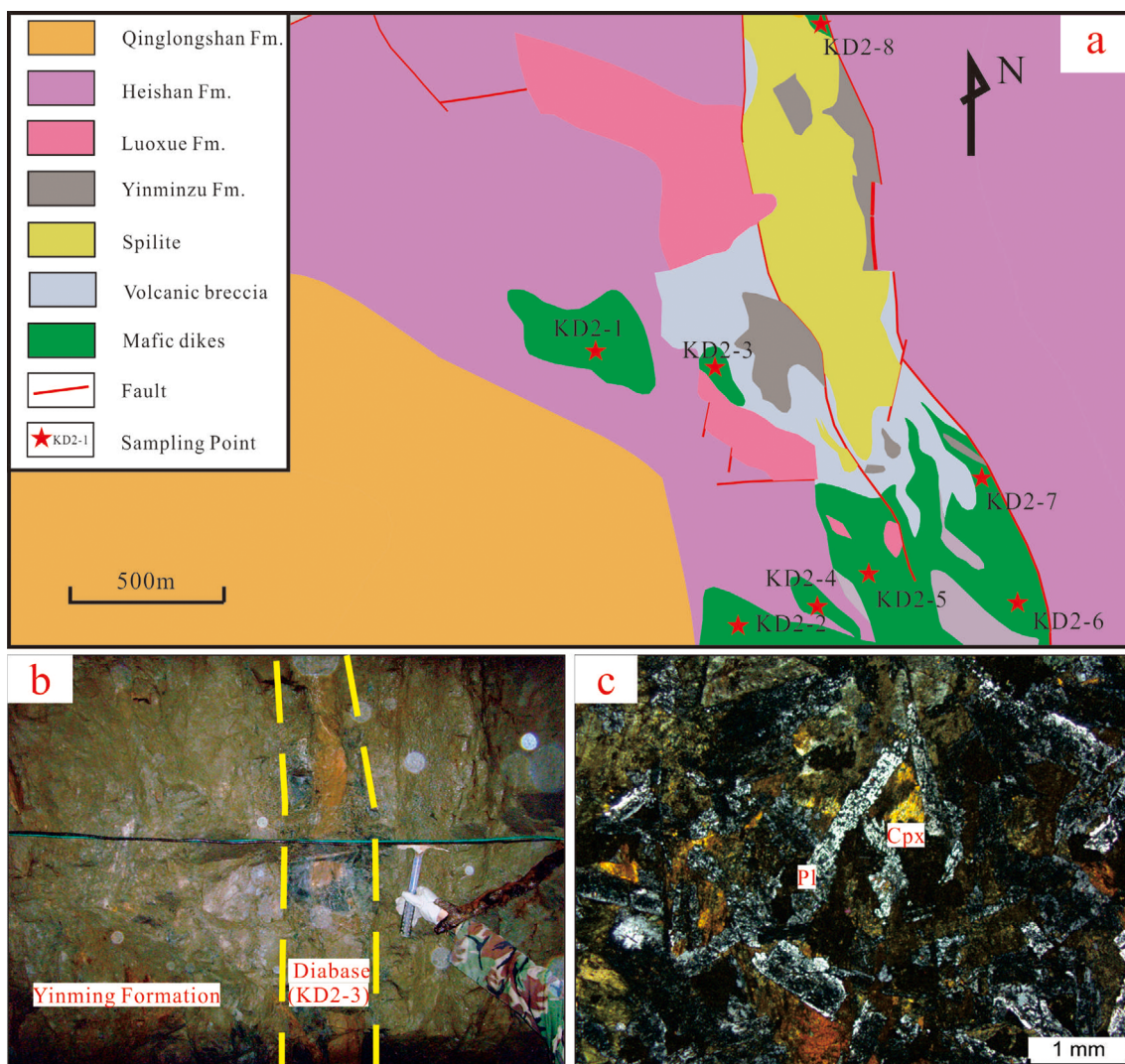


**Fig. 2.** (a) Geologic map of Yaopengzi area; (b) Field photographs of the dolerite; (c) Microphotograph of the dolerite (Pl: Plagioclase; Cpx: Clinopyroxene).

### 3. ANALYTICAL METHODS

The dolerite samples KD2-1 (intruding the Heishan Formation) and KD2-5 (intruding the Yinmin Formation) were chosen for zircon U-Pb dating and Hf isotope analysis. The samples were crushed/milled, and heavy minerals were separated by conventional methods (magnetic separation, sieving separation and heavy liquid separation) and hand-picked under a binocular microscope. Transparent zircons with good crystal shape and with no fractures were mounted on epoxy and solidified in an oven ( $60^{\circ}$ ) for 12h. The zircons were then polished until their centers were exposed. Cathodoluminescence (CL) imaging of zircons was conducted at the State Key Laboratory of Ore Deposit Geochemistry, Institute of Geochemistry, Chinese Academy of Sciences (GIGCAS), using a JSM-7800F field emission scanning electron microscope (SEM) with a MonoCL4 CL microscopy system. The zircon grains and spots for the U-Pb dating and Hf isotope analysis were chosen based on their representativeness observed under reflected and transmitted light microscopy and CL imaging.

In situ zircon U-Pb dating was conducted at the State Key Laboratory of Ore Deposit Geochemistry (GIGCAS), using an Agilent 7700x ICP-MS coupled with a GeoLasPro 193 nm Excimer laser ablation system. Analytical conditions: Energy density:  $10 \text{ J/cm}^2$ ; Beam diameter:  $44 \mu\text{m}$ ; Frequency: 5 Hz. The samples were ablated for 60s with the laser generator before sending into the ICP-MS with they as the carrier gas. 91500 zircon was used as a standard for isotopic fractionation calibration. NIST SRM 610 was used as an external standard for isotopic calculation, whilst  $^{29}\text{Si}$  was used as an internal standard. Common Pb correction followed the method outlined in Andersen (2002), whilst the analytical theory and processes were as outlined in Jackson et al. (2004). Primary data reduction was performed using ICPMS DataCal (Liu et al., 2010), and zircon isotopic age

and concordia diagram were calculated/drawn using Isoplot 3.0 (Ludwig, 2003).

In situ zircon Hf isotope analysis was conducted at the State Key Laboratory for Mineral Deposits Research, Nanjing University, using a UP193-FX 193-nm solid state laser ablation system coupled with an Element II MC-ICP-MS. Analytical conditions: Beam diameter:  $35 \mu\text{m}$ ; Frequency: 8 Hz. The samples were ablated for 60s with the laser generator before sending into the ICP-MS in a He carrier gas mixed with argon. Detailed operational and analytical processes were as outlined in Hou et al. (2007).

Whole-rock major and trace element analyses were conducted on eight dolerite samples at the ALS Geochemistry (Guangzhou). Major elements were measured using a PANalytical AXIOS XRF spectrometer, with analytical precision less than 5%. Trace elements were measured using an Agilent VISTA ICP-OES and Agilent 7700x ICP-MS, with analytical precision less than 10%. REEs were measured by a Perkin Elmer Elan 9000 ICP-MS, with analytical precision less than 10%.

## 4. RESULTS

### 4.1. Zircon U-Pb Age

In this study, 16 and 15 zircon grains were picked from KD2-1 and KD2-5, respectively. The zircons are white or pale yellow,  $15\text{--}120 \mu\text{m}$  long (length: width ratio: 2:1–4:1). CL images show weak/no oscillatory zoning, nor growth zoning or residual core (Fig. 3). Results of the zircon U-Pb dating were listed in Table 1. Concentrations of Th and U are  $104.732\text{--}696.110 \text{ ppm}$  and  $132.447\text{--}661.097 \text{ ppm}$ , respectively, whilst Th/U values are 0.63–1.14. Zircon  $^{207}\text{Pb}/^{206}\text{Pb}$  U-Pb ages of KD2-1 and KD2-5 were calculated to be  $1513 \pm 8.7 \text{ Ma}$  (MSWD = 0.021; n = 16) and  $1515 \pm 9.3 \text{ Ma}$  (MSWD = 0.021; n = 15), respectively (Fig. 3).

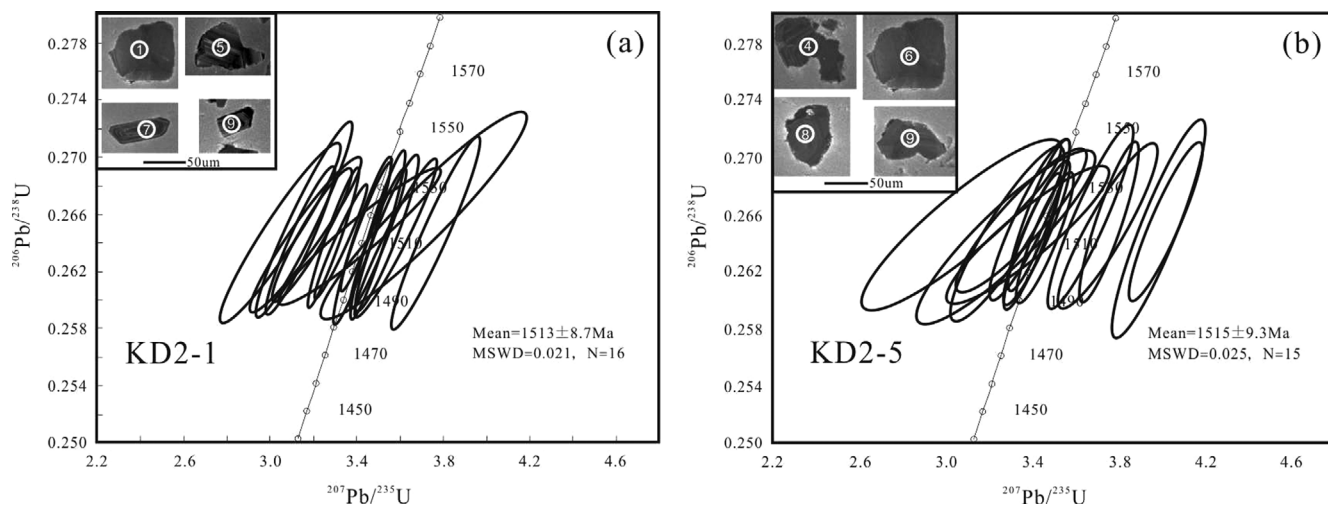


**Fig. 3.** (a) CL images of zircons from the dolerites. (b) U-Pb concordia diagram for zircons from the dolerites.

**Table 1.** LA-ICP-MS U-Pb isotope analysis results for zircons for the diabases from the Yaopengzi area

| Sample   | $\omega/10^{-6}$  |                  | $^{232}\text{Th}/^{238}\text{U}$ |           | $^{207}\text{Pb}/^{206}\text{Pb}$ |            | $^{207}\text{Pb}/^{235}\text{U}$ |          | $^{206}\text{Pb}/^{238}\text{U}$ |          | $^{207}\text{Pb}/^{206}\text{Pb}$ |          | $^{207}\text{Pb}/^{235}\text{U}$ |          | $^{206}\text{Pb}/^{238}\text{U}$ |  |
|----------|-------------------|------------------|----------------------------------|-----------|-----------------------------------|------------|----------------------------------|----------|----------------------------------|----------|-----------------------------------|----------|----------------------------------|----------|----------------------------------|--|
|          | $^{232}\text{Th}$ | $^{238}\text{U}$ | Ratio                            | $\sigma$  | Ratio                             | $\sigma$   | Ratio                            | $\sigma$ | t/Ma                             | $\sigma$ | t/Ma                              | $\sigma$ | t/Ma                             | $\sigma$ |                                  |  |
| KD2-1-1  | 293.172           | 284.042          | 1.03                             | 0.0934736 | 0.002374                          | 3.42713487 | 0.090515                         | 0.263859 | 0.003802                         | 1498     | 48                                | 1511     | 21                               | 1510     | 19                               |  |
| KD2-1-2  | 400.297           | 354.910          | 1.13                             | 0.0950249 | 0.002225                          | 3.49942368 | 0.087879                         | 0.264251 | 0.003271                         | 1529     | 44                                | 1527     | 20                               | 1512     | 17                               |  |
| KD2-1-3  | 344.525           | 547.686          | 0.63                             | 0.0949741 | 0.001962                          | 3.49955261 | 0.084441                         | 0.264537 | 0.003926                         | 1528     | 39                                | 1527     | 19                               | 1513     | 20                               |  |
| KD2-1-4  | 104.732           | 134.688          | 0.78                             | 0.0962401 | 0.002484                          | 3.53831628 | 0.096159                         | 0.264444 | 0.003771                         | 1554     | 248                               | 1536     | 22                               | 1513     | 19                               |  |
| KD2-1-5  | 399.744           | 350.387          | 1.14                             | 0.0931786 | 0.002029                          | 3.44133666 | 0.076207                         | 0.265345 | 0.003169                         | 1492     | 41                                | 1514     | 17                               | 1517     | 16                               |  |
| KD2-1-6  | 243.350           | 282.444          | 0.86                             | 0.0895717 | 0.002164                          | 3.29522509 | 0.079275                         | 0.264376 | 0.003236                         | 1417     | 46                                | 1480     | 19                               | 1512     | 16                               |  |
| KD2-1-7  | 242.861           | 289.191          | 0.84                             | 0.0902864 | 0.002199                          | 3.32646517 | 0.078982                         | 0.264044 | 0.002643                         | 1431     | 47                                | 1487     | 19                               | 1510     | 13                               |  |
| KD2-1-8  | 186.487           | 178.801          | 1.04                             | 0.1016537 | 0.003361                          | 3.76687455 | 0.135752                         | 0.264626 | 0.004449                         | 1655     | 61                                | 1586     | 29                               | 1513     | 23                               |  |
| KD2-1-9  | 435.733           | 555.996          | 0.78                             | 0.0968947 | 0.003061                          | 3.58680197 | 0.124959                         | 0.264555 | 0.003543                         | 1565     | 64                                | 1547     | 28                               | 1513     | 18                               |  |
| KD2-1-10 | 206.207           | 258.411          | 0.8                              | 0.0859284 | 0.002811                          | 3.14290335 | 0.107775                         | 0.264158 | 0.003395                         | 1337     | 63                                | 1443     | 26                               | 1511     | 17                               |  |
| KD2-1-11 | 223.728           | 287.680          | 0.78                             | 0.087146  | 0.003099                          | 3.19198758 | 0.124585                         | 0.26456  | 0.003023                         | 1365     | 69                                | 1455     | 30                               | 1513     | 15                               |  |
| KD2-1-12 | 115.225           | 145.970          | 0.79                             | 0.0867689 | 0.00376                           | 3.16131744 | 0.150173                         | 0.265672 | 0.004486                         | 1355     | 84                                | 1448     | 37                               | 1519     | 23                               |  |
| KD2-1-13 | 355.977           | 449.014          | 0.79                             | 0.0866102 | 0.003932                          | 3.1668832  | 0.168829                         | 0.264465 | 0.003575                         | 1352     | 88                                | 1449     | 41                               | 1513     | 18                               |  |
| KD2-1-14 | 140.801           | 197.318          | 0.71                             | 0.084106  | 0.004506                          | 3.04684192 | 0.188336                         | 0.264587 | 0.004192                         | 1295     | 104                               | 1419     | 47                               | 1513     | 21                               |  |
| KD2-1-15 | 265.736           | 269.266          | 0.99                             | 0.0931399 | 0.005689                          | 3.41050258 | 0.247977                         | 0.26444  | 0.003148                         | 1500     | 115                               | 1509     | 57                               | 1513     | 16                               |  |
| KD2-1-16 | 363.853           | 345.697          | 1.05                             | 0.1001006 | 0.00693                           | 3.71154007 | 0.315873                         | 0.265867 | 0.004804                         | 1628     | 129                               | 1574     | 68                               | 1520     | 24                               |  |
| KD2-5-1  | 122.961           | 154.698          | 0.79                             | 0.0838756 | 0.006048                          | 3.03347329 | 0.257645                         | 0.265047 | 0.003942                         | 1300     | 145                               | 1416     | 65                               | 1516     | 20                               |  |
| KD2-5-2  | 332.437           | 394.004          | 0.84                             | 0.0888838 | 0.005536                          | 3.20900895 | 0.23421                          | 0.264172 | 0.003982                         | 1411     | 120                               | 1459     | 57                               | 1511     | 20                               |  |
| KD2-5-3  | 199.985           | 217.329          | 0.92                             | 0.0901476 | 0.004877                          | 3.28912056 | 0.208427                         | 0.264438 | 0.003236                         | 1429     | 103                               | 1478     | 49                               | 1513     | 17                               |  |
| KD2-5-4  | 696.110           | 661.097          | 1.05                             | 0.0890611 | 0.003964                          | 3.2653708  | 0.169194                         | 0.265375 | 0.003299                         | 1406     | 85                                | 1473     | 40                               | 1517     | 17                               |  |
| KD2-5-5  | 379.097           | 341.749          | 1.11                             | 0.087405  | 0.003473                          | 3.20830635 | 0.147846                         | 0.264512 | 0.004037                         | 1369     | 72                                | 1459     | 36                               | 1513     | 21                               |  |
| KD2-5-6  | 105.913           | 132.447          | 0.8                              | 0.0991952 | 0.003729                          | 3.60466056 | 0.132786                         | 0.265072 | 0.003797                         | 1609     | 69                                | 1551     | 29                               | 1516     | 19                               |  |
| KD2-5-7  | 170.907           | 190.187          | 0.9                              | 0.0890938 | 0.002693                          | 3.29695517 | 0.105632                         | 0.265472 | 0.003716                         | 1406     | 59                                | 1480     | 25                               | 1518     | 19                               |  |
| KD2-5-8  | 274.036           | 367.434          | 0.75                             | 0.0906137 | 0.001994                          | 3.35513309 | 0.073023                         | 0.264245 | 0.003006                         | 1439     | 42                                | 1494     | 17                               | 1512     | 15                               |  |
| KD2-5-9  | 227.872           | 289.714          | 0.79                             | 0.0976282 | 0.002232                          | 3.60673373 | 0.075776                         | 0.265369 | 0.003696                         | 1589     | 43                                | 1551     | 17                               | 1517     | 19                               |  |
| KD2-5-10 | 140.959           | 164.631          | 0.86                             | 0.0901371 | 0.002331                          | 3.33468951 | 0.079926                         | 0.265775 | 0.003486                         | 1429     | 44                                | 1489     | 19                               | 1519     | 18                               |  |
| KD2-5-11 | 132.952           | 161.052          | 0.83                             | 0.0899722 | 0.002313                          | 3.32369295 | 0.086492                         | 0.26441  | 0.003463                         | 1425     | 49                                | 1487     | 20                               | 1512     | 18                               |  |
| KD2-5-12 | 192.209           | 254.912          | 0.75                             | 0.0897386 | 0.002174                          | 3.30760131 | 0.075831                         | 0.264105 | 0.003031                         | 1420     | 46                                | 1483     | 18                               | 1511     | 15                               |  |
| KD2-5-13 | 220.749           | 280.700          | 0.79                             | 0.1032573 | 0.002534                          | 3.83060466 | 0.097556                         | 0.2653   | 0.003651                         | 1684     | 45                                | 1599     | 21                               | 1517     | 19                               |  |
| KD2-5-14 | 426.300           | 500.354          | 0.85                             | 0.1024948 | 0.002839                          | 3.80450011 | 0.123046                         | 0.264802 | 0.005048                         | 1670     | 51                                | 1594     | 26                               | 1514     | 26                               |  |
| KD2-5-15 | 497.689           | 437.396          | 1.14                             | 0.0950197 | 0.002768                          | 3.53527039 | 0.11031                          | 0.265682 | 0.004217                         | 1529     | 55                                | 1535     | 25                               | 1519     | 21                               |  |

## 4.2. Zircon Hf Isotopes

Hafnium-isotope analysis results of the 8 and 9 zircons from KD2-1 and KD2-5 were listed in Table 2. The zircons contain  $^{176}\text{Lu}/^{177}\text{Hf} = 0.00128\text{--}0.00506$ ,  $^{176}\text{Hf}/^{177}\text{Hf} = 0.28192\text{--}0.28203$ , and mainly positive (except for four analyses)  $\varepsilon_{\text{Hf(t)}}$  ( $-0.3$  to  $5.3$ ). Single-stage zircon Hf model ages ( $t_{\text{DM1}}$ ) range  $1767\text{--}1961$  Ma (average: 1892 Ma), whilst two-stage zircon Hf model ages ( $t_{\text{DM2}}$ ) range  $4784\text{--}5071$  Ma (average: 4944 Ma).

## 4.3. Whole-rock Geochemistry

Whole-rock geochemical results for the eight Yaopengzi dolerite samples were listed in Table 3. The low  $\text{SiO}_2$  contents (44.31–49.04%; average: 46.62%) suggest that the rocks are

mafic. The rocks contain  $\text{TiO}_2 = 1.75\text{--}2.87\%$  (average: 2.39%),  $\text{Na}_2\text{O} = 2.79\text{--}4.84\%$  (average: 3.88%),  $\text{K}_2\text{O} = 0.26\text{--}3.57\%$  (average: 1.47%) and  $\text{Mg}^{\#} = 38.32\text{--}50.26$ . On the  $\text{Zr}/(\text{TiO}_2 \times 10000)\text{-Nb/Y}$  (Fig. 4a; Winchester and Floyd, 1977) and TAS classification diagrams (Fig. 4b; Cox et al., 1979), most samples fall into the alkaline basalt and alkaline gabbro fields, indicating that the Yaopengzi dolerite belongs to the alkaline basalt series.

The Yaopengzi dolerite contains relatively low total rare earth element ( $\Sigma\text{REE}$ ) contents (86.05–138.35 ppm) and moderate REE fractionation ( $\text{La}_{\text{N}}/\text{Yb}_{\text{N}} = 3.40\text{--}8.93$ ). In the chondrite-normalized REE diagram (Fig. 4c), the rocks show LREE enrichment and no discernible Eu and Ce anomalies. In the primitive mantle-normalized trace element diagram (Fig. 4d), the rocks show a right-inclining pattern, enrichments in large ion lithophile elements (LILEs) and distinct negative Sr anomalies.

**Table 2.** Zircon Hf isotope compositions for the diabases from Yaopengzi region

| Sample   | $^{176}\text{Hf}/^{177}\text{Hf}$ | $\sigma$ | $^{176}\text{Yb}/^{177}\text{Hf}$ | $\sigma$ | $^{176}\text{Lu}/^{177}\text{Hf}$ | $\sigma$ | $\varepsilon_{\text{Hf}}(t)^{(a)}$ | $T_{\text{DM1}}(\text{Ma})^{(b)}$ | $T_{\text{DM2}}(\text{Ma})^{(c)}$ |
|----------|-----------------------------------|----------|-----------------------------------|----------|-----------------------------------|----------|------------------------------------|-----------------------------------|-----------------------------------|
| KD2-1-01 | 0.28194                           | 0.000032 | 0.08237                           | 0.001482 | 0.00253                           | 0.000046 | 1.6                                | 1922                              | 5014                              |
| KD2-1-10 | 0.28198                           | 0.000025 | 0.07350                           | 0.000354 | 0.00239                           | 0.000011 | 3.1                                | 1863                              | 4922                              |
| KD2-1-11 | 0.28185                           | 0.000021 | 0.04024                           | 0.000508 | 0.00126                           | 0.000009 | -0.2                               | 1979                              | 5239                              |
| KD2-1-12 | 0.28197                           | 0.000024 | 0.09205                           | 0.000296 | 0.00291                           | 0.000014 | 2.4                                | 1894                              | 4929                              |
| KD2-1-13 | 0.28199                           | 0.000024 | 0.09168                           | 0.000279 | 0.00304                           | 0.000007 | 2.7                                | 1882                              | 4896                              |
| KD2-1-14 | 0.28203                           | 0.000062 | 0.09091                           | 0.002679 | 0.00278                           | 0.000046 | 4.5                                | 1807                              | 4784                              |
| KD2-1-15 | 0.28188                           | 0.000032 | 0.07003                           | 0.001394 | 0.00221                           | 0.000041 | -0.3                               | 1996                              | 5178                              |
| KD2-1-16 | 0.28200                           | 0.000050 | 0.10350                           | 0.002264 | 0.00336                           | 0.000076 | 2.8                                | 1882                              | 4866                              |
| KD2-5-07 | 0.28192                           | 0.000038 | 0.03814                           | 0.000133 | 0.00128                           | 0.000006 | 2.2                                | 1884                              | 5063                              |
| KD2-5-08 | 0.28184                           | 0.000044 | 0.07265                           | 0.002011 | 0.00243                           | 0.000073 | -1.8                               | 2059                              | 5270                              |
| KD2-5-09 | 0.28194                           | 0.000025 | 0.09574                           | 0.001550 | 0.00290                           | 0.000057 | 1.2                                | 1943                              | 5017                              |
| KD2-5-10 | 0.28192                           | 0.000048 | 0.06662                           | 0.000504 | 0.00211                           | 0.000016 | 1.3                                | 1932                              | 5071                              |
| KD2-5-11 | 0.28187                           | 0.000024 | 0.06793                           | 0.000515 | 0.00220                           | 0.000023 | -0.3                               | 1997                              | 5182                              |
| KD2-5-12 | 0.28201                           | 0.000055 | 0.16270                           | 0.002213 | 0.00506                           | 0.000037 | 1.7                                | 1950                              | 4822                              |
| KD2-5-13 | 0.28193                           | 0.000098 | 0.08863                           | 0.000783 | 0.00286                           | 0.000018 | 0.8                                | 1961                              | 5052                              |
| KD2-5-14 | 0.28193                           | 0.000041 | 0.06965                           | 0.000761 | 0.00209                           | 0.000027 | 1.8                                | 1911                              | 5035                              |
| KD2-5-15 | 0.28202                           | 0.000050 | 0.05395                           | 0.001038 | 0.00173                           | 0.000039 | 5.3                                | 1767                              | 4806                              |

Note: The  $^{176}\text{Hf}/^{177}\text{Hf}$  and  $^{176}\text{Lu}/^{177}\text{Hf}$  ratios of chondrite and depleted mantle at the present are 0.282772 and 0.0332, 0.28325 and 0.0384;  $(^{176}\text{Lu}/^{177}\text{Hf})_{\text{LC}} = 0.019$ ;  $\lambda = 1.867 \times 10^{-11} \text{ year}^{-1}$ ;  $t$  = crystallization time of zircon.

$$^{(a)}\varepsilon_{\text{Hf}}(t) = \{[(^{176}\text{Hf}/^{177}\text{Hf})_{\text{S}} - (^{176}\text{Lu}/^{177}\text{Hf})_{\text{S}} \times (e^{\lambda t} - 1)] / [(^{176}\text{Hf}/^{177}\text{Hf})_{\text{CHUR}} - (^{176}\text{Lu}/^{177}\text{Hf})_{\text{CHUR}} \times (e^{\lambda t} - 1)] - 1\} \times 10000.$$

$$^{(b)}T_{\text{DM1}} = 1/\lambda \ln \{[(^{176}\text{Hf}/^{177}\text{Hf})_{\text{S}} - (^{176}\text{Hf}/^{177}\text{Hf})_{\text{DM}}] / [(^{176}\text{Lu}/^{177}\text{Hf})_{\text{S}} - (^{176}\text{Lu}/^{177}\text{Hf})_{\text{DM}}] + 1\}.$$

$$^{(c)}T_{\text{DM2}} = t + 1/\lambda \ln \{[(^{176}\text{Hf}/^{177}\text{Hf})_{\text{S}} - (^{176}\text{Hf}/^{177}\text{Hf})_{\text{DM}}] / [(^{176}\text{Lu}/^{177}\text{Hf})_{\text{LC}} - (^{176}\text{Lu}/^{177}\text{Hf})_{\text{DM}}] + 1\}.$$

## 5. DISCUSSION

### 5.1. Ages of Dolerite Formation

Zircons from the Yaopengzi dolerite show weak oscillatory zoning (Wu and Zheng, 2004; Wang et al., 2013a), no corrosive margin and high Th/U values ( $> 0.4$ ), resembling typical magmatic (esp. mafic) zircons. Therefore, the U-Pb concordia ages at  $1513 \pm 8.7 \text{ Ma}$  (KD2-1) and  $1515 \pm 9.3 \text{ Ma}$  (KD2-5) reflect the Yaopengzi dolerite crystallization ages. Mafic rocks are also exposed in the Zhuqing and Tong'anzen–Bajiaoxiang areas in the SW margin of the Yangtze block (Fig. 5). The Zhuqing gabbro was SIMS U-Pb dated to be  $1494 \pm 6 \text{ Ma}$  for zircon,  $1486 \pm 3 \text{ Ma}$  and  $1490 \pm 4 \text{ Ma}$  for baddeleyite (Fan et al., 2013), whilst the Tong'anzen–Bajiao gabbro-diorite was LA-ICP-MS zircon U-Pb dated to be  $1513 \pm 21 \text{ Ma}$  (Geng et al., 2012). This indicates that the early Mesoproterozoic mafic intrusions are widely exposed in the Huili area (SW margin of the Yangtze block), with the ages coeval with the Columbia supercontinent breakup (ca. 1.6–1.2 Ga).

### 5.2. Petrogenesis

Mafic rocks are widely considered to be products of mantle-derived basaltic magmatism and associated with regional extension (Williams et al., 2001; Mathieu et al., 2008), and thus represent an important evidence to understand deep-level mantle

composition and evolution (Langmuir et al., 1992; Depaolo and Ellen Daley, 2000; Polat et al., 2002; Niu and O'Hara, 2003; Niu, 2008). We discussed the nature of the magma source and the possible tectonic setting based on the reported new data in petrology, whole-rock geochemistry and Hf isotopes for the Yaopengzi dolerite.

#### 5.2.1. Alteration influence on minerals

Alteration appears to be minor in hand specimen and under the microscope, which is also supported by their LOI (1.75–3.72%; Table 3)  $> 1.5\%$  (Lin et al., 2006). In mafic and ultramafic rocks, high field strength elements (e.g., Zr) are largely immobile under low–medium grade metamorphism (Wood, 1979; Barnes et al., 1985). In Figure 6, it is shown that Zr displays good positive correlations with other HFSEs (Th, Y, Nb, Ta, Hf) and REEs, suggesting that these elements are immobile and can be used to trace the primary rock geochemistry (Pearce, 1975; Wood et al., 1979; Rudnick et al., 1985; Kerrich et al., 1999; Polat and Hofmann, 2003; Li et al., 2016; Wu et al., 2017). Major elements (esp. K and Na) appear to be more affected by late-stage alteration, yet the similar results shown in the Zr/TiO<sub>2</sub> versus Nb/Y and TAS classification diagrams (Figs. 4a and b) suggest that the major elements can still reflect the primary rock geochemistry. In this study, major element geochemistry is only used in rock type classification and in discussing fractional crystallization processes.

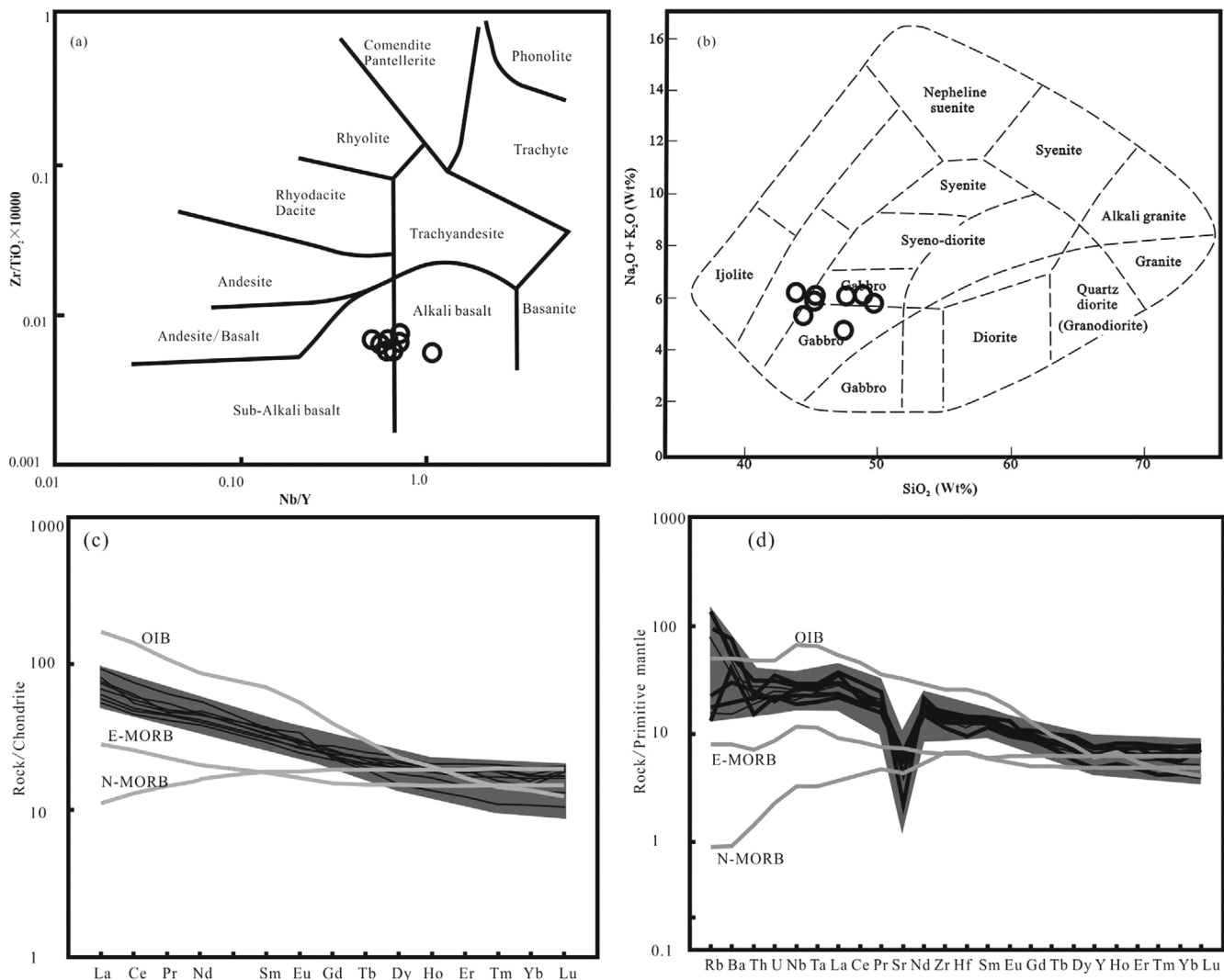


**Fig. 4.** (a)  $Zr/TiO_2 \times 1000$  versus  $Nb/Y$  diagrams of the Yaopengzi dolerites (modified from Winchester and Floyd, 1977); (b)  $SiO_2$  versus  $Na_2O + K_2O$  (Wt%) diagrams of the Yaopengzi dolerites (modified from Cox et al., 1979); (c) Chondrite-normalized REE pattern of the Yaopengzi dolerites (normalizing values from Sun and Macdonough, 1989); (d) Primitive mantle-normalized incompatible element spider diagram for normalized incompatible element spider diagram (normalizing values from Sun and Macdonough, 1989).

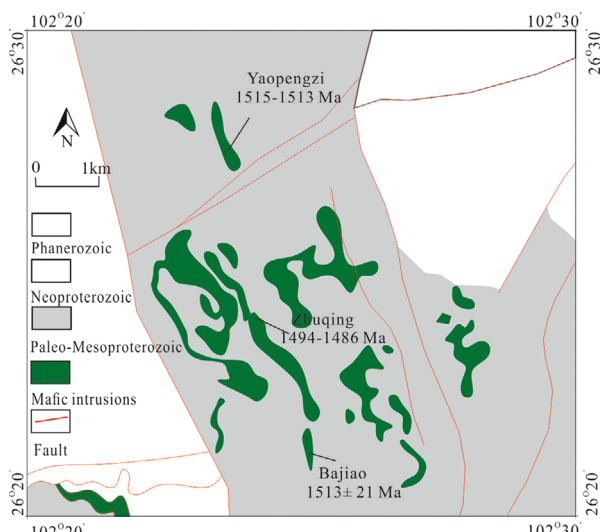


**Fig. 5.** Simplified geological map of the Mesoproterozoic to earliest Neoproterozoic rocks in the Tong'an region (modified from Fan et al., 2013).

### 5.2.2. Tectonic setting of the dolerite formation

The DF1-DF2 diagram, which uses a combination of immobile element indices ( $\ln(La/Th)$ ,  $\ln(Sm/Th)$ ,  $\ln(Yb/Th)$  and  $\ln(Nb/Th)$ ) (Agrawal et al., 2008), can effectively (78–97% accuracy) (Yang, 2014) discriminate the tectonic settings of mafic rocks, including altered ones. In this diagram (Figs. 7a–d), all the Yaopengzi dolerite samples fall into the oceanic island basalt (OIB) and continental rift basalt (CRB) fields. In the  $2Nb-Zr/4-Y$  ternary diagram (Fig. 7e), all samples fall into the within-plate basalt (WPB) field. The samples fall into the intraplate rift alkaline basalt and mantle plume basalt fields in the  $Zr-Zr/Y$  diagram (Fig. 7f). We concluded that the Yaopengzi dolerite was likely formed in mantle plume-related continental rift setting.

There are many evidences that support the rift setting in the western margin of the Yangtze block: (1) Considering the Mesoproterozoic basin evolution features of the Huili area, the

**Table 3.** Major (%) and trace element (ppm) analyses of diabases from the Yaopengzi area

| Sample                             | KD2-1 | KD2-2 | KD2-3  | KD2-4 | KD2-5 | KD2-6 | KD2-7 | KD2-8 |
|------------------------------------|-------|-------|--------|-------|-------|-------|-------|-------|
| SiO <sub>2</sub>                   | 44.31 | 47.69 | 46.54  | 44.73 | 49.04 | 45.83 | 46.12 | 48.73 |
| TiO <sub>2</sub>                   | 2.87  | 2.46  | 2.36   | 2.52  | 1.75  | 2.41  | 2.65  | 2.08  |
| Al <sub>2</sub> O <sub>3</sub>     | 15.3  | 13.91 | 14.51  | 14.21 | 13.53 | 14.21 | 14.32 | 13.60 |
| Fe <sub>2</sub> O <sub>3</sub>     | 18.56 | 14.79 | 14.69  | 15.45 | 15.39 | 18.99 | 15.61 | 14.05 |
| MnO                                | 0.08  | 0.22  | 0.18   | 0.13  | 0.25  | 0.18  | 0.12  | 0.22  |
| MgO                                | 5.82  | 6.89  | 6.23   | 6.03  | 7.44  | 6.56  | 6.64  | 7.17  |
| CaO                                | 2.28  | 6.54  | 9.51   | 7.9   | 4.21  | 3.52  | 6.12  | 5.83  |
| Na <sub>2</sub> O                  | 2.79  | 4.45  | 3.46   | 3.13  | 4.84  | 3.85  | 3.97  | 4.56  |
| K <sub>2</sub> O                   | 3.57  | 0.89  | 0.52   | 2.05  | 0.26  | 1.87  | 1.74  | 0.85  |
| P <sub>2</sub> O <sub>5</sub>      | 0.46  | 0.23  | 0.22   | 0.36  | 0.21  | 0.33  | 0.25  | 0.27  |
| LOI <sup>(a)</sup>                 | 3.72  | 1.75  | 1.92   | 3.32  | 2.98  | 2.07  | 2.45  | 2.35  |
| Total                              | 99.76 | 99.82 | 100.14 | 99.83 | 99.48 | 99.82 | 99.99 | 99.71 |
| Mg# <sup>(b)</sup>                 | 38.32 | 47.99 | 45.66  | 43.60 | 48.92 | 40.63 | 45.73 | 50.26 |
| Sc                                 | 25    | 41    | 39     | 33    | 42    | 33    | 35    | 43    |
| V                                  | 275   | 414   | 474    | 366   | 374   | 352   | 386   | 347   |
| Cr                                 | 107   | 123   | 104    | 96    | 136   | 124   | 113   | 132   |
| Co                                 | 44    | 51    | 49     | 48    | 55    | 48    | 53    | 72    |
| Ni                                 | 80    | 92    | 91     | 89    | 100   | 92    | 98    | 104   |
| Cu                                 | 14    | 64    | 127    | 72    | 7     | 13    | 65    | 39    |
| Zn                                 | 42    | 89    | 53     | 54    | 122   | 81    | 74    | 105   |
| Ga                                 | 24.9  | 18.4  | 20.8   | 22.9  | 18.3  | 20.1  | 21.7  | 18.7  |
| Rb                                 | 59.5  | 11.3  | 14.3   | 87.9  | 8.2   | 84.3  | 49.5  | 9.9   |
| Sr                                 | 46.3  | 126.8 | 136.5  | 90.4  | 119   | 84    | 110   | 124   |
| Y                                  | 21.9  | 33.5  | 34.6   | 28.1  | 29.5  | 26.1  | 31.2  | 32.6  |
| Zr                                 | 157   | 147   | 168    | 168   | 126   | 144   | 156   | 139   |
| Nb                                 | 20.6  | 16.1  | 18.5   | 19.6  | 13.3  | 17.1  | 17.9  | 14.6  |
| Cs                                 | 12.25 | 0.28  | 0.37   | 6.28  | 0.18  | 6.23  | 3.25  | 0.26  |
| Ba                                 | 537   | 134   | 203    | 350   | 269   | 309   | 240   | 105   |
| La                                 | 25.4  | 16.1  | 22.6   | 20.6  | 14.6  | 20.2  | 18.4  | 15.8  |
| Ce                                 | 53.1  | 34.4  | 36.9   | 43.45 | 31.8  | 41.7  | 39.2  | 33.3  |
| Pr                                 | 6.84  | 4.94  | 5.08   | 5.04  | 4.40  | 5.8   | 5.2   | 4.9   |
| Nd                                 | 29.50 | 21.70 | 23.20  | 25.40 | 20.10 | 24.3  | 23.9  | 21.1  |
| Sm                                 | 6.27  | 5.49  | 6.33   | 6.10  | 5.05  | 5.72  | 5.85  | 5.28  |
| Eu                                 | 2.20  | 1.71  | 1.78   | 1.79  | 1.60  | 1.96  | 1.85  | 1.77  |
| Gd                                 | 5.31  | 5.68  | 6.53   | 5.82  | 5.25  | 5.26  | 5.72  | 5.43  |
| Tb                                 | 0.79  | 0.94  | 1.07   | 0.91  | 0.87  | 0.81  | 0.95  | 0.89  |
| Dy                                 | 4.20  | 6.26  | 6.88   | 5.34  | 5.71  | 4.94  | 5.82  | 6.07  |
| Ho                                 | 0.85  | 1.19  | 1.32   | 1.12  | 1.14  | 1.04  | 1.18  | 1.21  |
| Er                                 | 2.25  | 3.49  | 3.91   | 3.54  | 3.16  | 2.68  | 3.57  | 3.36  |
| Tm                                 | 0.31  | 0.54  | 0.59   | 0.45  | 0.48  | 0.43  | 0.52  | 0.56  |
| Yb                                 | 2.04  | 3.33  | 3.77   | 2.73  | 3.08  | 2.54  | 3.04  | 3.18  |
| Lu                                 | 0.29  | 0.54  | 0.57   | 0.53  | 0.48  | 0.38  | 0.55  | 0.49  |
| Hf                                 | 4.1   | 3.9   | 4.5    | 4.1   | 3     | 3.5   | 4.1   | 3.7   |
| Ta                                 | 1.2   | 0.9   | 1      | 1.1   | 0.8   | 1.1   | 1.0   | 1.0   |
| Pb                                 | 2     | 4     | 4      | 2     | 2     | 2     | 3     | 3     |
| Th                                 | 1.91  | 1.82  | 2.17   | 2.65  | 1.27  | 1.58  | 2.27  | 1.56  |
| U                                  | 0.52  | 0.46  | 0.43   | 0.67  | 0.46  | 0.51  | 0.56  | 0.47  |
| Zr/Nb                              | 7.6   | 9.1   | 9.1    | 8.6   | 9.5   | 8.4   | 8.7   | 9.5   |
| La/Nb                              | 1.2   | 1.0   | 1.2    | 1.1   | 1.1   | 1.2   | 1.0   | 1.1   |
| Th/La                              | 0.1   | 0.1   | 0.1    | 0.1   | 0.1   | 0.1   | 0.1   | 0.1   |
| Th <sub>PM</sub> /Ta <sub>PM</sub> | 0.8   | 1.0   | 0.8    | 0.9   | 0.9   | 0.8   | 0.9   | 0.9   |
| La <sub>PM</sub> /Nb <sub>PM</sub> | 0.8   | 0.9   | 0.7    | 0.9   | 0.9   | 0.9   | 0.9   | 1.1   |

<sup>(a)</sup>LOI: loss on ignition.<sup>(b)</sup>Mg# = 100 × molar MgO/(Mg + FeO<sub>T</sub>), assuming FeO<sub>T</sub> = FeO + 0.9 × Fe<sub>2</sub>O<sub>3</sub>, Total iron as FeO<sub>T</sub>.

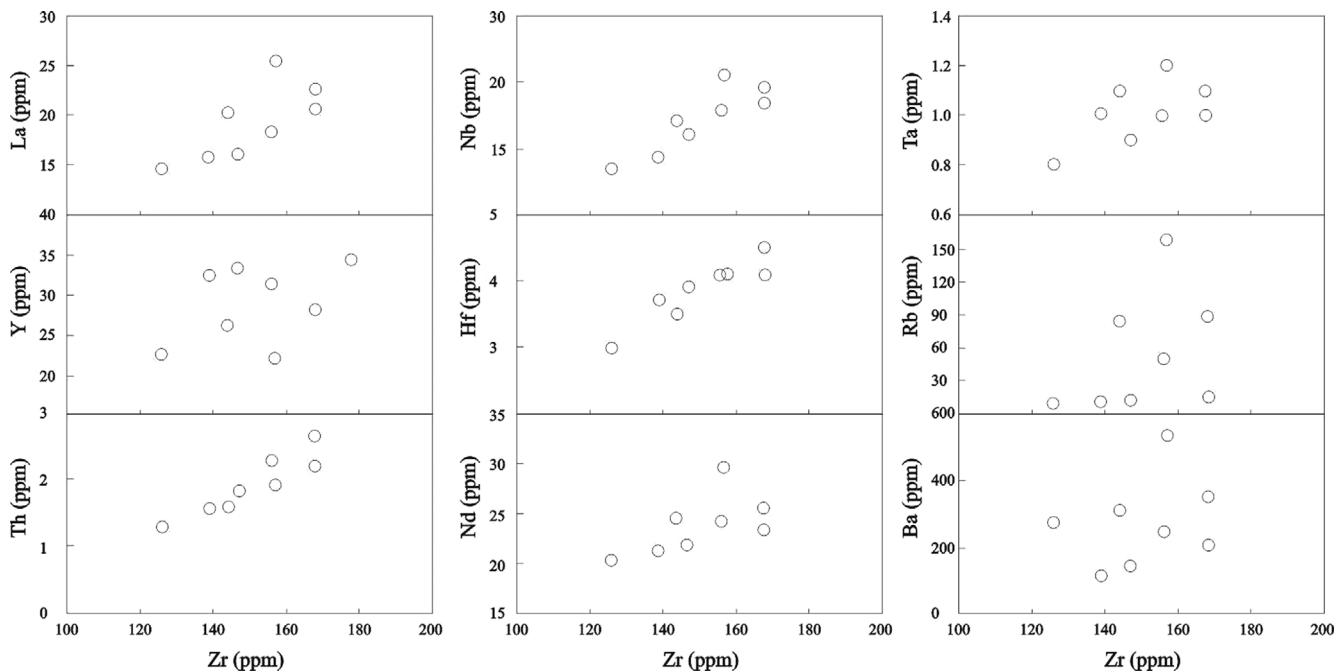


**Fig. 6.** Diagrams of La, Y, Th, Nb, Hf, Nd, Ta, Rb, and Ba versus Zr to evaluate the mobility of these elements during alteration.

Heishan Formation (Dongchuan Group) contains a narrow range of rock types, which comprise mainly black carbonaceous (Wang et al., 2014), silty and tuffaceous sediments deposited in a reducing environment. The rocks show a complete continental shelf-continental slope-continental shelf sedimentary cycle, indicating an extensional passive continental margin setting with volcanic graben features; (2) Wang et al. (2018) investigates carbonates belonging to the Luoxue and Luzhijiang formations of the Dongchuan Group, and obtain Sr isotopic ratios. Both the upper Luoxue and Luzhijiang carbonates have  $^{87}\text{Sr}/^{86}\text{Sr}$  higher than expected for contemporaneous seawater, which indicate that Luoxue and Luzhijiang carbonates were deposited in a rift-related basin; (3) The Zhuqing magmatic Fe-Ti-V oxide ore deposits are typically hosted in mafic-ultramafic (ca.  $1494 \pm 6$  Ma), plume-related layered intrusions or large igneous provinces (Fan et al., 2013); (4) The ca. 1.51 Ga Tong'an zhen-Bajiao gabbro-diorite mafic intrusions have been demonstrated to be formed in continental rift setting (Geng et al., 2012). Thus, the basic rocks of the western Yangtze should be interpreted as generation from mantle plume-related in a rift environment. Furthermore, these lines of evidence further support that the Yaopengzi dolerite was formed by the Mesoproterozoic continental rift-related magmatism in the western margin of the Yangtze block, coeval with the rifting-breakup event of the Columbia supercontinent (Rogers and Santosh, 2002; Zhao et al., 2004; Peng et al., 2009; Evans and Mitchell, 2011; Silveira et al., 2012).

### 5.2.3. Fractional crystallization and crustal assimilation

The Yaopengzi dolerite samples contain low  $\text{Mg}^{\#}$  (38.32–50.26), Ni (80–104) and Cr (96–132; Table 3), indicating that the parental magma was not in equilibrium with mantle peridotite (Cox, 1980), but had experienced various degrees of fractional crystallization during its ascent or stalling in the magma chambers. In the Harker diagrams (Fig. 8),  $\text{MgO}$  correlates positively with  $\text{Al}_2\text{O}_3$ , Ni and Cr, implying clinopyroxene and olivine fractionation in the parental magma.

Different from typical continental mafic rocks, which are commonly influenced by crustal assimilation during the magma ascent and show complex geochemical characteristics, the Yaopengzi dolerite does not show distinct evidence of crustal assimilation: 1) The rocks are relatively LILE-rich and with no distinct HFSE (Nb, Ta and Hf) or negative Eu anomalies, and contain OIB-like REE fractionation pattern and primitive mantle-normalized trace element features; 2) In the Nb/Yb versus Th/Yb (Fig. 9a) and Nb/Yb versus  $\text{TiO}_2/\text{Yb}$  (Fig. 9b) discrimination diagrams, the samples fall inside/around the OIB field; 3) The crustal ( $\text{Nb}/\text{La})_{\text{PM}}$  and ( $\text{Ta}/\text{La})_{\text{PM}}$  values are  $\ll 1$  (Rudnick and David, 1995), whereas the samples contain  $(\text{Nb}/\text{La})_{\text{PM}} = 0.78\text{--}0.96$  (average: 0.87) and  $(\text{Ta}/\text{La})_{\text{PM}} = 0.74\text{--}1.06$  (average: 0.90); 4) The range of zircon  $\varepsilon_{\text{Hf}(t)}$  values is smaller than those typical of crustal contamination.

### 5.2.4. Magma source

Hafnium contains similar geochemical features with Zr and can replace the latter in zircons, leading to low Lu/Hf value (0.002).

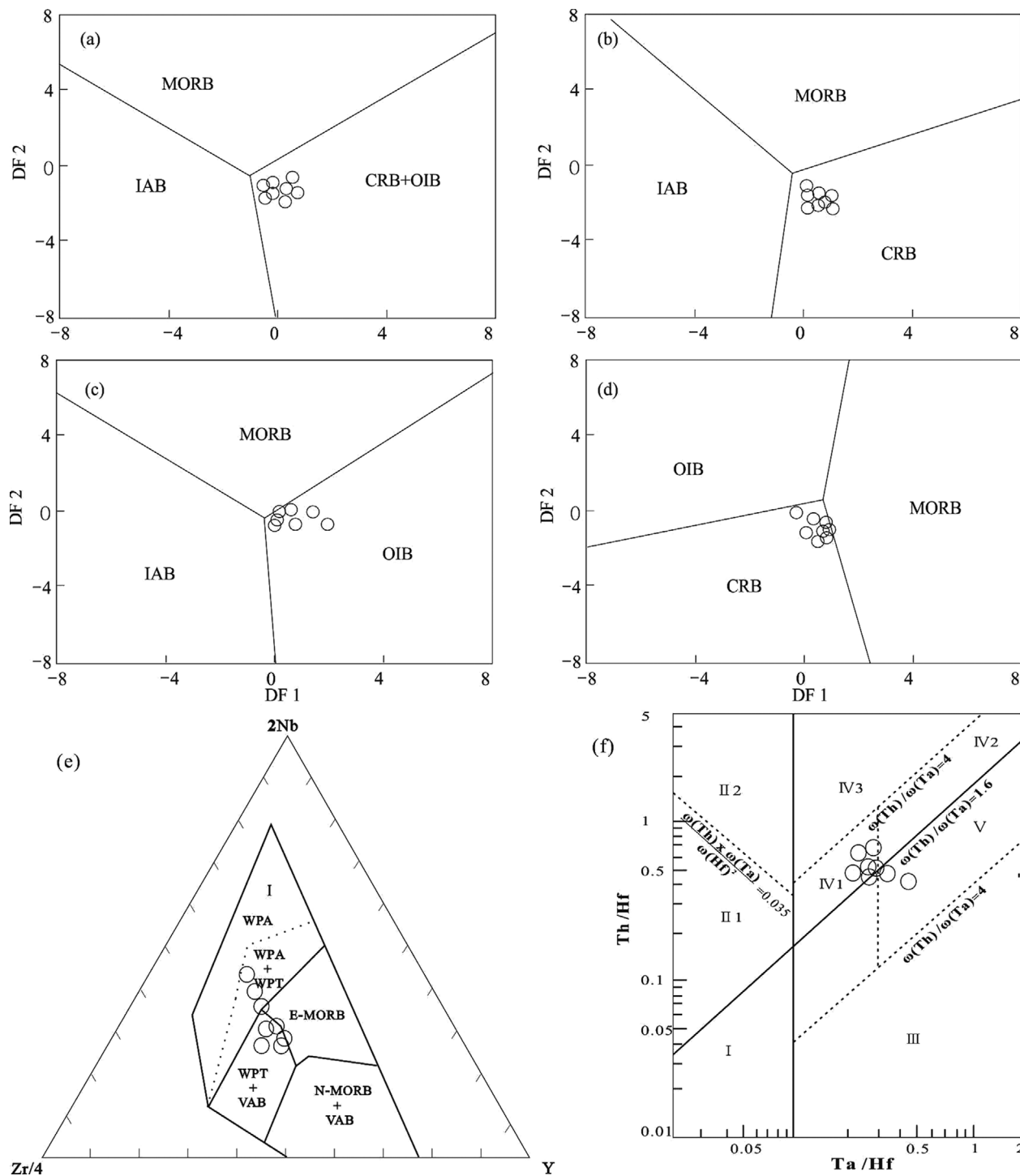


**Fig. 7.** Tectonic discrimination diagrams for the Yaopengzi dolerites: (a–d) Log-transformed immobile trace element tectonic discrimination diagrams; (e) 2Nb-Zr/4-Y diagram of spilites (modified from Winchester and Floyd, 1977); (f) Ta/Hf versus Th/Hf diagram of spilites (modified from Sun et al., 1989). Figure 7a:  $DF1 = 0.3518 \ln(La/Th) + 0.6013 \ln(Sm/Th) - 1.3450 \ln(Yb/Th) + 2.1056 \ln(Nb/Th) - 5.4763$ ,  $DF2 = -0.3050 \ln(La/Th) - 1.1801 \ln(Sm/Th) + 1.6189 \ln(Yb/Th) + 1.2260 \ln(Nb/Th) - 0.9944$ ; Figure 7b:  $DF1 = 0.3305 \ln(La/Th) + 0.3484 \ln(Sm/Th) - 0.9562 \ln(Yb/Th) + 2.0777 \ln(Nb/Th) - 4.5628$ ,  $DF2 = -0.1928 \ln(La/Th) - 1.1989 \ln(Sm/Th) + 1.7531 \ln(Yb/Th) + 0.6607 \ln(Nb/Th) - 0.4384$ ; Figure 7c:  $DF1 = 1.7517 \ln(Sm/Th) - 1.9508 \ln(Yb/Th) + 1.9573 \ln(Nb/Th) - 5.0928$ ,  $DF2 = -2.2412 \ln(Sm/Th) + 2.2060 \ln(Yb/Th) + 1.2481 \ln(Nb/Th) - 0.8243$ ; Figure 7d:  $DF1 = -0.5558 \ln(La/Th) - 1.4260 \ln(Sm/Th) + 2.2935 \ln(Yb/Th) - 0.6890 \ln(Nb/Th) + 4.1422$ ,  $DF2 = -0.9207 \ln(La/Th) + 3.6520 \ln(Sm/Th) - 1.9866 \ln(Yb/Th) + 1.0574 \ln(Nb/Th) - 4.4283$ ; MORB – Oceanic ridge basalt; IAB – Island arc tholeiite; OIB – Ocean island basalt; CRB – Continental rift basalt; WPA – Within Plate alkali basalt; WPT – Within Plate tholeiite; E-MORB – Enrichment mid-oceanic ridge basalt; N-MORB – Normal mid-oceanic ridge basalt; VAB – Volcanic arc basalt; I – the second district of the margin of divergent oceanic plate; II – Margin of convergent plate (II<sub>1</sub> – Oceanic island-arc basalt; II<sub>2</sub> – Continental margin arc basalt and continental marginal volcanic arc basalt); III – Oceanic plate interior(oceanic island basalt and seamount basalt, mid-oceanic ridge basalt); IV – Continental intraplate (IV<sub>1</sub> – Continental rift alkali basalt and margin of continental rift alkali basalt; IV<sub>2</sub> – Continental extension belt (early rift) basalt; IV<sub>3</sub> – Continental collision basalt); V – Mantle plume basalt.

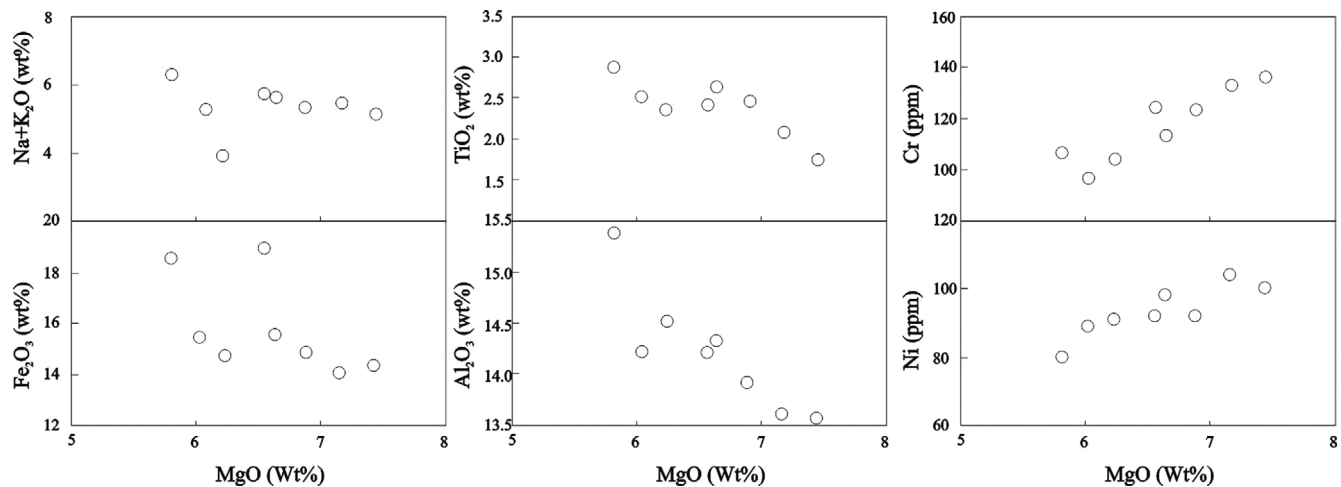


**Fig. 8.** Plots of MgO versus SiO<sub>2</sub>, TiO<sub>2</sub>, Cr, Fe<sub>2</sub>O<sub>3</sub>, Al<sub>2</sub>O<sub>3</sub> and Ni for the Yaopengzi dolerites.

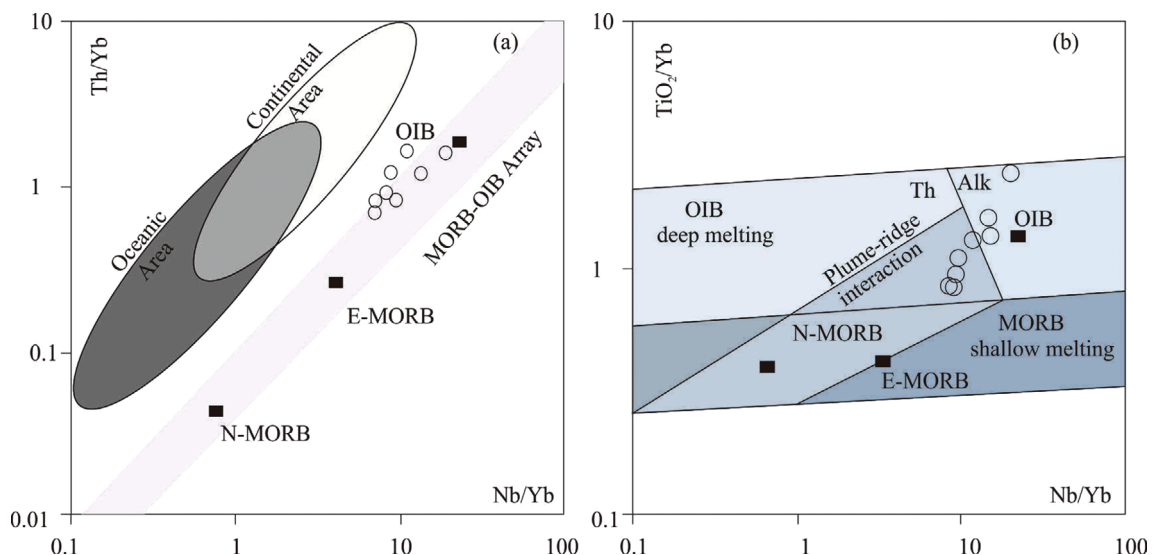


**Fig. 9.** Nb/Yb versus Th/Yb (a, modified from Pearce, 2014) and Nb/Yb versus TiO<sub>2</sub>/Yb (b, modified from Pearce, 2014) discrimination diagram for the Yaopengzi dolerites.

During <sup>176</sup>Lu decay, the accumulated <sup>176</sup>Hf/<sup>177</sup>Hf changes are commonly very small (< 0.0005). Igneous zircons from mafic magmas can effectively preserve the initial magmatic <sup>176</sup>Hf/<sup>177</sup>Hf ratio (Patchett et al., 1982), and thus unraveling the magmatic source nature and evolution (Blichert and Albarede, 1997; Knudsen et al., 2001; Kinny et al., 2003; Beloisova et al., 2006; Wu et al., 2007). Zircons from the Yaopengzi dolerite contain  $\epsilon_{\text{Hf(t)}}$  values (-1.8 – 5.3) that lie between the average depleted mantle and lower crust, suggesting that the magma may have sourced from mixing between the enriched/depleted mantle and the crust (Fig. 10). Nevertheless, the Yaopengzi doleritic magma was unlikely to be significantly crustal contaminated as aforementioned, and thus the source may have been enriched mantle derived.

Ratios of REEs and HFSEs with similar fractionation coefficients are controlled by the degree/depth of partial melting (of the magma source) but not by fractional crystallization, and can

thus be used to differentiate the magma sources (Pearce, 2008). From Table 3, the HFSE ratios (Zr/Nb, La/Nb) are (7.6–9.5) and (1.0–1.2), respectively, which are within the enriched mantle range (Weaver, 1991).

Whole-rock geochemistry and zircon Hf-isotopes of the early Mesoproterozoic Yaopengzi dolerite clearly demonstrate that the mantle source may have been enriched mantle. Although both mantle plume and continental subduction-related crust-mantle processes can generate enriched mantle characteristics, the Yaopengzi doleritic magma was more likely sourced from the former, due to: 1) Th<sub>PM</sub>/Ta<sub>PM</sub> = 0.77–1.16 (average: 0.97), La<sub>PM</sub>/Nb<sub>PM</sub> = 0.88–1.28 (average: 1.08), resembling those of typical mantle plume-related basalts (Th<sub>PM</sub>/Ta<sub>PM</sub> < 1, La<sub>PM</sub>/Nb<sub>PM</sub> < 1; Neal et al., 2002; Guo et al., 2014); 2) From the HFSE ratios of Nb/Th, Zr/Nb, Nb/Y and Zr/Y (Figs. 11a and b), the Yaopengzi samples fall around the enriched (EN) and primitive (PM) mantle

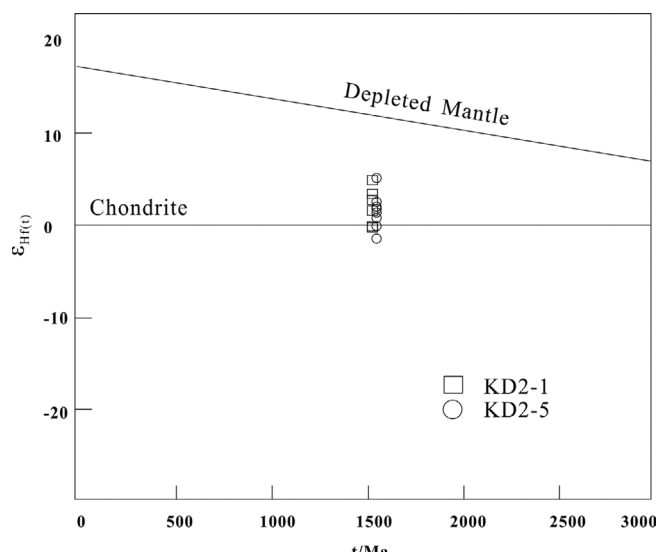


**Fig. 10.** Plot of zircon  $\epsilon_{\text{Hf}(t)}$  versus U-Pb ages of zircons from the Yaopengzi dolerites.

fields and trend towards the deep depleted mantle (DEP), a trend similar to that of Paleoproterozoic mantle plume-related basalts (Condie, 2005); 3) In tectonic discrimination diagram (Figs. 7f and 9b), some of the Yaopengzi samples fall into the mantle plume field.

For semi-quantitative determination of the partial melting conditions of the parental magma source, we adopted the bulk silicate earth (BSE)-normalized Gd/Yb versus La/Yb diagram proposed by Reichow et al. (2005). The three curves in the La/Yb versus Gd/Yb diagram (Fig. 11c) represent the non-model batch partial melting of primitive mantle composition-bearing spinel peridotite (SP) and garnet peridotite (GP) (below 3 GPa) and garnet peridotite (GP) (below 4 GPa). The Yaopengzi dolerite data points fall along the garnet peridotite (3 GPa) curve, with some of them having low degree of partial melting (< 10%). Since the spinel-garnet transition occurs at 2.8–3.1 GPa or 60–80 km deep (Wilson, 1993; Robinson and Wood, 1998), we

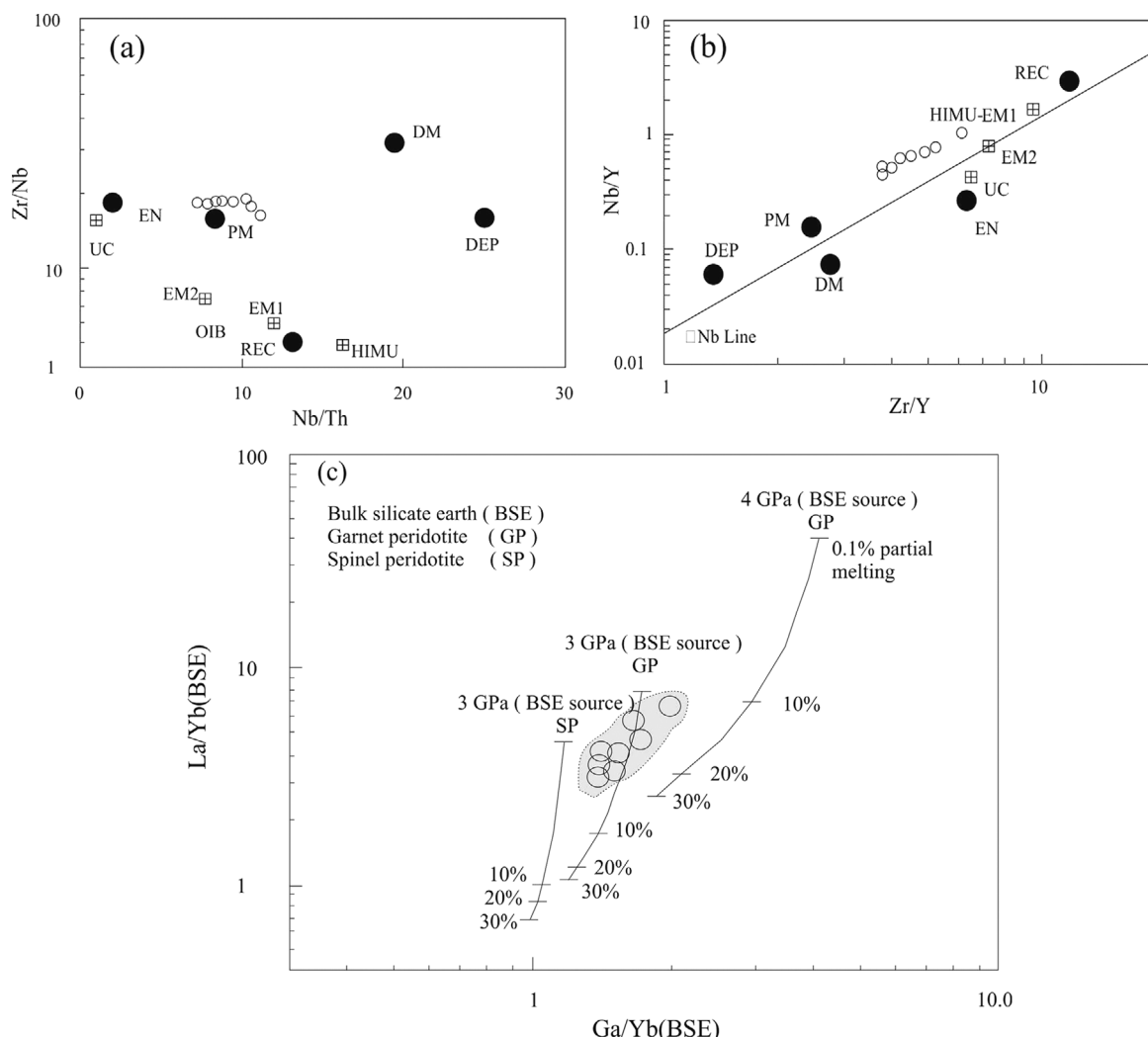


**Fig. 11.** The determination diagrams of magma source for the Yaopengzi dolerites: (a) Nb/Th versus Zr/Nb; (b) Zr/Y versus Nb/Y diagrams (Distribution of the early Mesoproterozoic dolerite ( $\text{SiO}_2 \leq 56\%$ ) from Yaopengzi; modified from Condie, 2005); (c) La/Yb versus Gd/Yb diagram (normalized to bulk silicate earth: McDonough and Sun, 1995; modified from Reichow, 2005).

postulated that the parental magma of the Yaopengzi dolerite was generated deep in the garnet stability field (> 80 km) of the rising mantle plume.

In summary, the Yaopengzi dolerite was likely formed in a continental rift setting. Its parental magma may have originated from the rising mantle plume deep in the garnet stability field (> 80 km), and have undergone fractional crystallization and possible weak crustal assimilation during its ascent.

### 5.3. Tectonic Significance

Present understanding in the relationships between the Yangtze block and the Columbia supercontinent is highly limited (Rogers and Santosh, 2002; Zhao et al., 2004). Recent studies suggested that the Yangtze block was influenced by the Paleo-Mesoproterozoic Columbian tectonic evolution, as evidenced by: 1) Archean basement is present in the Yangtze block, as supported by the oldest zircon age ( $3300.8 \pm 8.4$  Ma) of the Kongling complex in the northern margin of the Yangtze block (Zhang et al., 2006b; Yang et al., 2008), the numerous Archean detrital zircons in the Precambrian strata (Zhao et al., 2010; Wang et al., 2013b), and the Archean xenocrystic zircons in the Paleozoic lamprophyres (Zheng et al., 2006; Zhang et al., 2016); 2) During the Columbia assembly stage (ca. 2.1–1.8 Ga), collisional orogenic-related thermotectonic ages (ca. 2.0–1.8 Ga) were reported in various places in the Yangtze block (Zhang et al., 2006a; Wu et al., 2008; Peng et al., 2009; Wu et al., 2009; Xiong et al., 2009; Zhang et al., 2011), and orogenic-related UHT granulite was formed in the northern margin of the block (Hu et al., 2012; Lei et al., 2014); 3) During the post-collisional extension stage (ca. 1.8–1.6 Ga), the northern and SW margins of the Yangtze block have developed a series of anorogenic bimodal magmatism (Zhao et al., 2010; Wang et al., 2013a; Wang et al., 2014a; Yang, 2014).

During the post-collisional extension stage (ca. 1.8–1.6 Ga), the northern and SW margins of the Yangtze block have developed a series of anorogenic bimodal magmatism (Zhao et al., 2010; Wang et al., 2013a; Wang et al., 2014; Yang, 2014). For example, the ca. 1.73 Ga Haizi granite porphyry (Wang et al., 2013c), the ca. 1.72 Ga Hekou quartz keratophyre (Wang et al., 2012), the ca. 1.7 Ga Dahongshan tuff (Zhao et al., 2010) and the ca. 1.69 Ga Tongan diabase dykes (Liu et al., 2018). This ca. 1.7 Ga magmatism was considered as the main feature of the typical rift. We interpreted that the Yangtze block once experienced the continental rift setting at ca. 1.7 Ga and began to breakup from the Columbia supercontinent.

During the Columbia breakup (ca. 1.6–1.2 Ga), extensive anorogenic magmatism had occurred on various continents of the world, e.g., America, Baltic, Eastern India, Siberia and Western Australia (Åhäll et al., 2000; Roy et al., 2002; Goldberg, 2010;

Silveira et al., 2012; Teixeira et al., 2012; Ernst et al., 2013). Coeval magmatism in the Yangtze block was rarely reported in the past. In this study, combination with literature data (Geng et al., 2012; Fan et al., 2013), we revealed that the ca. 1.5 Ga magmatism in the Huili area (western margin of the Yangtze block) shows distinct mantle plume characteristics, and was likely products of continental rifting. This ca. 1.5 Ga continental rifting-related magmatism in the Yangtze block was unlikely to be an isolated event but part of a global one. For instance, extensive ca. 1.5 Ga magmatism was documented in Angola and Congo of the Archean Congo craton (Silveira et al., 2012; Ernst et al., 2013), and ca. 1.5 Ga dykes were represented in the central Anabar shield (Ernst et al., 2000), and ca. 1.52 Ga granite and rhyolite were documented within the south India rift and the basins around it (Patranabis, 2003). In addition, ca. 1.5 Ga mafic dyke swam was reported in São Francisco Craton of South America (Silveira et al., 2012). These magmatic activities were likely mantle plume-related (Rogers and Santosh, 2002; Zhao et al., 2004; Peng et al., 2009; Evans and Mitchell, 2011; Silveira et al., 2012), and represent the surficial expressions of the deep earth geodynamics of the Columbia breakup. Therefore, the Yangtze block is likely to be part of the Columbia supercontinent.

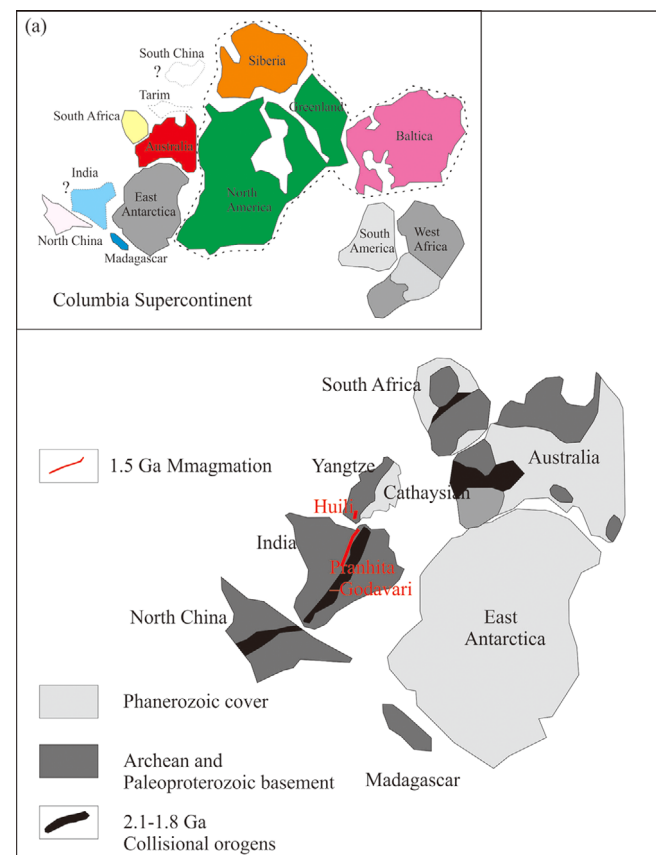


**Fig. 12.** Possible position of the Yangtze Block in the Columbia supercontinent reconstructed by Zhao et al. (2002) and Zhou et al. (2004).

Recently, Zhao et al. (2002), Wang et al. (2013b) and Zhou et al. (2014) have presented a comprehensive investigation for the location of the Yangtze block in the Columbia supercontinent. Due to the lack of geological and paleomagnetic information, the location is loosely constrained to be either the northwestern part (near the Siberia, North America and Tarim blocks; Zhao et al., 2011) or western part (near South Africa, India and Australia blocks; Wang et al., 2013b) of the supercontinent. As aforementioned, ca. 1.5 Ga mantle plume-related magmatism was widespread in the India, Congo-São Francisco and Siberia blocks. A ca. 1.5 Ga reconstruction of northern Siberian Craton adjacent to Congo-São Francisco Craton based on coeval widespread magmatism events (Ernst et al., 2013). With that information, we supported that the Yangtze block was more likely situated in western Columbia (Fig. 12), and proposed that there may have been a super plume in this region at ca. 1.5 Ga, which led to the regional continental rifting and associated magmatism, and the eventual breakup of the Columbia supercontinent.

## 6. CONCLUSION

- 1) Zircon U-Pb age dating of the Yaopengzi dolerite yielded 1515–1513 Ma, indicating intensive early Mesoproterozoic mafic magmatism in the Huili area.
- 2) Trace element geochemistry indicates that the Yaopengzi dolerite was formed in a mantle plume-related intracontinental rift setting.

3) Major and trace element geochemistry and zircon Hf isotopes indicate that the Yaopengzi dolerite belongs to the alkaline basalt series. The magma source contains enriched mantle features, and the parental magma may have been sourced from the deep ascending mantle plume in the garnet stability field ( $> 80$  km). It was likely that the magma had undergone fractional crystallization during its ascent, with minor crustal contamination in the continental lithosphere, associated with the breakup of the Columbia supercontinent.

## ACKNOWLEDGMENTS

This study was financially supported by the National Basic Research Program of China (No. 2014CB440901), the National Natural Science Foundation of China (Project No. 51608192), and the Natural Science Foundation of Hunan Province (Grant No. 2016JJ4031).

## REFERENCES

- Åhäll, K.I., Connelly, J.N., and Brewer, T.S., 2000, Episodic rapakivi magmatism due to distal orogenesis? Correlation of 1.69–1.50 Ga orogenic and inboard, “anorogenic” events in the Baltic Shield. *Geology*, 28, 823–826.
- Agrawal, S., Guevara, M., and Verma, S.P., 2008, Tectonic discrimination of basic and ultrabasic volcanic rocks through log-transformed ratios of immobile trace elements. *International Geology Review*, 50, 1057–1079.
- Andersen, T., 2002, Correction of common lead in U-Pb analyses that do not report  $^{204}\text{Pb}$ . *Chemical Geology*, 192, 59–79.
- Barnes, S.J., Naldrett, A.J., and Gorton, M.P., 1985, The origin of the fractionation of platinum-group elements in Terrestrial magmas. *Chemical Geology*, 53, 303–323.
- Beloisova, B.A., Griffin, W.L., and O'Reilly, S.Y., 2006, Zircon crystal morphology, trace element signatures and Hf isotope composition as a tool for petrogenetic modeling: examples from Eastern Australian granitoids. *Journal of Petrology*, 47, 329–353.
- Blichert, J. and Albarene, F., 1997, The Lu-Hf isotope geochemistry of chondrites and the evolution of the mantle-crust system. *Earth and Planetary Science Letters*, 148, 243–258.
- Condie, K.C., 2005, High field strength element ratios in Archean basalts: a window to evolving sources of mantle plumes? *Lithos*, 79, 491–504.
- Cox, K.G., Bell, J.D., and Pankhurst, R.J., 1979, *The Interpretation of Igneous Rocks*. Allen and Unwin, London, 450 p.
- Cox, K.G., 1980, A model for flood basalt volcanism. *Journal of Petrology*, 21, 629–650.
- Depaolo, D.J. and Daley, E.E., 2000, Neodymium isotopes in basalts of the southwest basin and range and lithospheric thinning during continental extension. *Chemical Geology*, 169, 157–185.
- Ernst, R.E., Buchan, K.L., Hamilton, M.A., Okrugin, A.V., and Tomshin, M.D., 2000, Integrated paleomagnetism and U-Pb geochronology of mafic dikes of the eastern Anabar shield region, Siberia: implications for Mesoproterozoic paleolatitude of Siberia and comparison with Laurentia. *The Journal of Geology*, 108, 381–401.
- Ernst, R.E., Pereira, E., Hamilton, M.A., Pisarevsky, S.A., Rodrigues, J., Tassinari, C.C.G., Teixeira, W., and Van-Dunem, V., 2013, Mesoproterozoic intraplate magmatic ‘barcode’ record of the Angola portion of the Congo craton: newly dated magmatic events at 1505 and 1110 Ma and implications for Nuna (Columbia) supercontinent reconstructions. *Precambrian Research*, 230, 103–118.
- Evans, D.A.D. and Mitchell, R.N., 2011, Assembly and breakup of the core of Paleoproterozoic–Mesoproterozoic supercontinent Nuna. *Geology*, 39, 443–446.
- Fan, H.P., Zhu, W.G., Li, Z.X., Zhong, H., Bai, Z.J., He, D.F., Chen, C.J., and Cao, C.Y., 2013, Ca. 1.5 Ga mafic magmatism in South China during the break-up of the supercontinent Nuna/Columbia: the Zhuqing Fe-Ti-V oxide ore-bearing mafic intrusions in western Yangtze Block. *Lithos*, 16, 85–98.
- Geng, Y.S., Liu, Y.Q., Gao, L.Z., Peng, N., and Jiang, X.J., 2012, Geochronology of the Mesoproterozoic Tong'an Formation in southwestern margin of Yangtze craton: new evidence from zircon LA-ICP-MS U-Pb ages. *Geological Journal of China Universities*, 86, 1479–1490. (in Chinese with English abstract)
- Goldberg, A.S., 2010, Dyke swarms as indicators of major extensional events in the 1.9–1.2 Ga Columbia supercontinent. *Journal of Geodynamics*, 50, 176–190.

- Guo, Y., Wang, S.W., Sun, X.M., Yang, B., Liao, Z.W., Zhou, B.G., Jiang, X.F., Hou, L., and Yang, B., 2014, The Paleoproterozoic breakup event in the southwest Yangtze Block: evidence from U-Pb zircon age and geochemistry. *Acta Geologica Sinica*, 88, 1652–1665. (in Chinese with English abstract)
- Hou, K.J., Li, Y.H., Zou, T.R., Qu, X.M., Shi, Y.R., and Xie, G.Q., 2007, Laser ablation-MC-ICP-MS technique for Hf isotope microanalysis of zircon and its geological applications. *Acta Petrologica Sinica*, 23, 2595–2604. (in Chinese with English abstract)
- Hu, Z.C., Liu, Y.S., Gao, S., Liu, W.G., Zhang, W., Tong, X.R., Lin, L., Zong, K.Q., Li, M., Chen, H.H., Zhou, L., and Yang, L., 2012, Improved in situ Hf isotope ratio analysis of zircon using newly designed X skimmer cone and Jet sample cone in combination with the addition of nitrogen by laser ablation multiple collector ICPMS. *Journal of Analytical Atomic Spectrometry*, 27, 1391–1399.
- Jackson, S.E., Pearson, N.J., and Griffin, W.L., 2004, The application of laser ablation-inductively coupled plasma-mass spectrometry to in situ U-Pb zircon geochronology. *Chemical Geology*, 211, 47–69.
- Kerrick, R., Polat, A., Wyman, D., and Hollings, P., 1999, Trace element systematics of Mg-, to Fe-tholeiitic basalt suites of the Superior Province: implications for Archean mantle reservoirs and greenstone belt genesis. *Lithos*, 46, 163–187.
- Kinny, P.D. and Maas, R., 2003, Lu-Hf and Sm-Nd isotope systems in zircon. *Reviews in Mineralogy and Geochemistry*, 53, 327–341.
- Knudsen, T.L., Griffin, W., Hartz, E., Andresen, A., and Jackson, S., 2001, In-situ hafnium and lead isotope analyses of detrital zircons from the Devonian sedimentary basin of NE Greenland: a record of repeated crustal reworking. *Contributions to Mineralogy and Petrology*, 141, 83–94.
- Langmuir, C.H., Klein, E.M., and Plank, T., 1992, Petrological systematics of mid-ocean ridge basalts: constraints on melt generation beneath ocean ridges. *Mantle Flow and Melt Generation at Mid-ocean Ridges*, 71, 183–280.
- Li, H., Xi, X.S., Sun, H.S., Kong, H., Wu, Q.H., Wu, C.M., and Gabo-Ratio, J.A.S., 2016, Geochemistry of the Batang Group in the Zhaokalong area, Yushu, Qinghai: implications for the Late Triassic tectonism in the northern Sanjiang region, China. *Acta Geologica Sinica (English Edition)* 90, 704–721.
- Lei, H.C., Xiang, H., Zhang, Z.M., Qi, M., Dong, X., and Lin, Y.H., 2014, Paleoproterozoic UHT granulite in the Sulu orogen and its tectonic implications. *Acta Petrologica Sinica*, 30, 2435–2445. (in Chinese with English abstract)
- Lin, G.C., Li, X.H., and Li, W.X., 2006, SHRIMP U-Pb zircon geochronology, geochemistry and Nd-Hf isotope of Neoproterozoic magmatic rocks in western Sichuan: petrogenesis and tectonic significance. *Science in China (Series D Earth Sciences)*, 07, 630–645.
- Liu, Y.S., Hu, Z.C., Zong, K.Q., Gao, C.G., Gao, S., and Xu, J., 2010, Reappraisal and refinement of zircon U-Pb isotope and trace element analyses by LA-ICP-MS. *Chinese Science Bulletin*, 55, 83–93.
- Ludwig, K.R., 2003, User's manual for Isoplot/Ex Version 3.0: a geochronological toolkit for Microsoft Excel. Berkeley Geochronology Center Special Publication, Berkeley, 74 p.
- Liu, W., Yang, X.Y., Shu, S.Y., Liu, L., and Yuan, S.H., 2018, Precambrian basement and Late Paleoproterozoic to Mesoproterozoic tectonic evolution of the SW Yangtze Block, South China: constraints from zircon U-Pb dating and Hf Isotopes. *Minerals*, 8, 333. <https://doi.org/10.3390/min8080333>
- Mathieu, L., Vries, B.V.W.D., Holohan, E.P., and Troll, V.P., 2008, Dykes, cups, saucers and sills: analogue experiments on magma intrusion into brittle rocks. *Earth and Planetary Science Letters*, 271, 1–13.
- McDonough, W.F. and Sun, S.S., 1995, The composition of the Earth. *Chemical Geology*, 120, 223–253.
- Neal, C.R., Mahoney, J.J., and Chazey, W.J., 2002, Mantle sources and the highly variable role of continental lithosphere in basalt petrogenesis of the Kerguelen Plateau and Broken Ridge LIP: results from ODP Leg 183. *Journal of Petrology*, 43, 1177–1250.
- Niu, Y.L., 2008, The origin of alkaline lavas. *Science*, 320, 883–884.
- Niu, Y.L. and O'Hara, M.J., 2003, Origin of ocean island basalts: a new perspective from petrology, geochemistry, and mineral physics considerations. *Journal of Geophysical Research Solid Earth*, 108, 283–299.
- Patchett, P.J., Kouvo, O., Hedge, C.E., and Tatsumoto, M., 1982, Evolution of continental crust and mantle heterogeneity: evidence from Hf isotopes. *Contributions to Mineralogy and Petrology*, 78, 279–297.
- Patranabis, D.S., 2003, Proterozoic felsic volcanism in the Pranhita Godavari valley, India: its implication on the origin of the basin. *Journal of Asian Earth Sciences*, 21, 623–631.
- Pearce, J.A., 1975, Basalt geochemistry used to investigate past tectonic environments on Cyprus. *Tectonophysics*, 25, 41–67.
- Pearce, J.A., 2008, Geochemical fingerprinting of oceanic basalts with applications to ophiolite classification and the search for Archean oceanic crust. *Lithos*, 100, 14–48.
- Pearce, J.A., 2014, Immobile element fingerprinting of ophiolites. *Elements*, 10, 101–108.
- Peng, M., Wu, Y.B., Wang, J., Jiao, W.F., Liu, X.C., and Yang, S.H., 2009, Paleoproterozoic Mafic Dyke form Kongling Terrain in the Yangtze Craton and Its Implication. *Chinese Science Bulletin*, 54, 1098–1104.
- Peng, M., Wu, Y.B., Gao, S., Zhang, H.F., Wang, J., Liu, X.C., Gong, H.J., Zhou, L., Hu, Z.C., Liu, Y.S., and Yuan, H.L., 2012, Geochemistry, zircon U-Pb age and Hf isotope compositions of Paleoproterozoic aluminous A-type granites from the Kongling terrain, Yangtze Block: constraints on petrogenesis and geologic implications. *Gondwana Research*, 22, 140–151.
- Polat, A. and Hofmann, A.W., 2003, Alteration and geochemical patterns in the 3.7–3.8 Ga Isua greenstone belt, West Greenland. *Precambrian Research*, 126, 197–218.
- Polat, A., Hofmann, A.W., and Rosing, M.T., 2002, Boninite-like volcanic rocks in the 3.7–3.8 Ga Isua greenstone belt, West Greenland: geochemical evidence for intra-oceanic subduction zone processes in the early Earth. *Chemical geology*, 184, 231–254.
- Reichow, M.K., Saunders, A.D., White, R.V., Al'Mukhamedov, A.I., and Medvedev, A.Y., 2005, Geochemistry and petrogenesis of basalts from the west Siberian basin: an extension of the Permo-Triassic Siberian traps, Russia. *Lithos*, 79, 425–452.
- Robinson, J.A.C. and Wood, B.J., 1998, The depth of the spinel to garnet transition at the peridotite solidus. *Earth and Planetary Science Letters*, 164, 277–284.
- Rogers, J.J.W. and Santosh, M., 2002, Configuration of Columbia, a Mesoproterozoic Supercontinent. *Gondwana Research*, 5, 5–22.

- Roy, A., Sarkar, A., Jeyakumar, S., Aggrawal, S.K., and Ebihara, M., 2002, Mid-Proterozoic plume related thermal event in eastern Indian craton: evidence from trace elements, REE geochemistry and Sr-Nd isotope systematics of basic-ultrabasic intrusives from Dalma volcanic belt. *Gondwana Research*, 5, 133–146.
- Rudnick, R.L. and David, M.F., 1995, Nature and composition of the continental crust: a lower crustal perspective. *Reviews of Geophysics*, 33, 267–309.
- Rudnick, R.L., McClenann, S.M., and Taylor, S.R., 1985, Large ion lithophile elements in rocks from high-pressure granulite facies terrains. *Geochimica et Cosmochimica Acta*, 49, 1645–1655.
- Silveira, E.M., Söderlund, U., Oliveira, E.P., Ernst, R.E., and Menezes Leal, A.B., 2012, First precise U-Pb Baddeleyite ages of 1500 Ma mafic dykes from the São Francisco Craton, Brazil, and tectonic implications. *Lithos*, 174, 144–156.
- Sun, S.S. and Macdonough, W.F., 1989, Chemical and isotopic systematics of oceanic basalts: implications for mantle composition and processes. In: Saunders, A.D. and Norry, M.J. (eds.), *Magma in the Ocean Basins*. Geological Society, London, Special Publications, 42, p. 313–345.
- Sun, S.S., McDonough, W.F., and Ewart, A., 1989, Four component dynamic model for East Australian basalts. In: Johnson R.W. (ed.), *Intraplate Volcanism in Eastern Australia and New Zealand*. Cambridge University Press, Cambridge, p. 333–347.
- Teixeira, W., DAgrella-Filho, M.S., Ernst, R.E., Hamilton, M.A., Girardi, V.A.V., Mazzucchelli, M., and Bettencourt, J.S., 2012, U-Pb (ID-TIMS) baddeleyite ages and paleomagnetism of 1.79 and 1.59 Ga tholeiitic dyke swarms, and position of the Rio de la Plata Craton within the Columbia supercontinent. *Lithos*, 174, 157–174.
- Wager, L.R. and Brown, G.M., 1968, *Layered Igneous Rocks*. Oliver and Boyd, Edinburgh, 588 p.
- Wang, W. and Zhou, M.F., 2014a, Provenance and tectonic setting of the Paleo-Mesoproterozoic Dongchuan Group in the southwestern Yangtze Block, South China: implication for the breakup of the supercontinent Columbia. *Tectonophysics*, 610, 110–127.
- Wang, Q.H., Yang, H., Yang, D.B., and Xu, W.L., 2014b, Mid-Mesoproterozoic (similar to 1.32 Ga) diabase swarms from the western Liaoning region in the northern margin of the North China Craton: baddeleyite Pb-Pb geochronology, geochemistry and implications for the final breakup of the Columbia supercontinent. *Precambrian Research*, 254, 114–128.
- Wang, L.J., Griffin, W.L., Yu, J.H., and O'Reilly, S.Y., 2013b, U-Pb and Lu-Hf isotopes in detrital zircon from Neoproterozoic sedimentary rocks in the northern Yangtze Block: implications for Precambrian crustal evolution. *Gondwana Research*, 23, 1261–1272.
- Wang, D.B., Yin, F.G., Sun, Z.M., Wang, L.Q., Wang, B.D., Liao, S.Y., Tang, Y., and Ren, G.M., 2013a, Zircon U-Pb age and Hf isotope of Paleoproterozoic mafic intrusion on the western margin of the Yangtze Block and their implications. *Geological Bulletin of China*, 32, 617–630. (in Chinese with English abstract)
- Wang, W., Bolhar, R., Zhou, M.F., and Zhao, X.F., 2018, Enhanced terrestrial input into Paleoproterozoic to Mesoproterozoic carbonates in the southwestern South China Block during the fragmentation of the Columbia Supercontinent. *Precambrian Research*, 313, 1–17.
- Wang, Z., Guo, Y., Yang, B., Wang, S., Sun, X., Hou, L., Zhou, B., and Liao, Z., 2013c, Discovery of the 1.73 Ga Haizi anorogenic type granite in the western margin of Yangtze Craton, and its geological significance. *Acta Geologica Sinica-English edition*, 87, 931–942. (in Chinese with English abstract)
- Weaver, B.L., 1991, The origin of ocean island basalt end-member composition: trace element and isotopic constraints. *Earth and Planetary Science Letters*, 104, 381–397.
- Williams, H., Turner, S., Kelley, S., and Harris, N., 2001, Age and composition of dikes in Southern Tibet: new constraints on the timing of east-west extension and its relationship to postcollisional volcanism. *Geology*, 29, 339–342.
- Wilson, M., 1993, Magmatism and the geodynamics of basin formation. *Sedimentary Geology*, 86, 5–29.
- Winchester, J.A. and Floyd, P.A., 1977, Geochemical discrimination of different magma series and their differentiation products using immobile element. *Chemical Geology*, 20, 325–343.
- Wood, D.A., Joron, J.L., and Treuil, M., 1979, A re-appraisal of the use of trace elements to classify and discriminate between magma series erupted in different tectonic settings. *Earth and Planetary Science Letters*, 45, 326–336.
- Wu, Y. and Zheng, Y., 2004, Genesis of zircon and its constraints on interpretation of U-Pb age. *Chinese Science Bulletin*, 49, 1554–1569.
- Wu, F.Y., Li, X.H., Zheng, R.F., and Gao, S., 2007, Lu-Hf isotopic systematics and their applications in petrology. *Acta Petrologica China*, 02, 185–220. (in Chinese with English abstract)
- Wu, M.D., Duan, J.S., Song, X.L., Chen, L., and Dan, Y., 1990, *Geology of Kunyang Group in Yunnan Province*. Scientific Press of Yunnan Province, Kunming, 265 p. (in Chinese)
- Wu, Y.B., Zheng, Y.F., Gao, S., Jiao, W.F., and Liu, Y.S., 2008, Zircon U-Pb age and trace element evidence for Paleoproterozoic granulite facies metamorphism and Archean crustal rocks in the Dabie Orogen. *Lithos*, 101, 308–322.
- Wu, Y.B., Gao, S., Gong, H.J., Xiang, H., Jiao, W.F., Yang, S.H., Liu, Y.S., and Yuan, H.L., 2009, Zircon U-Pb age, trace element and Hf isotope composition of Kongling terrane in the Yangtze Craton: refining the timing of Paleoproterozoic high-grade metamorphism. *Journal of Metamorphic Geology*, 27, 461–477.
- Wu, J.H., Li, H., Xi, X.S., Kong, H., Wu, Q.H., Peng, N.L., Wu, X.M., Cao, J.Y., and Gabo-Ratio, J.A.S., 2017, Geochemistry and geochronology of the mafic dikes in the Taipusi area, northern margin of North China Craton: implications for Silurian tectonic evolution of the Central Asian Orogen. *Journal of Earth System Science*, 126, 64. <https://doi.org/10.1007/s12040-017-0841-z>
- Xiong, Q., Zheng, J.P., Yu, C.M., and Su, Y.P., 2009, Zircon U-Pb age and Hf isotope of Quanyishang A-type granite in Yichang: significance for the Yangtze continental cratonization in Paleoproterozoic. *Chinese Science Bulletin*, 54, 436–446.
- Yang, H., Liu, P.H., Meng, E., Wang, F., Xiao, L.L., and Liu, C.H., 2014, Geochemistry and its tectonic implications of metabasite in the Dahongshan Group in southwestern Yangtze block. *Acta Petrologica Sinica*, 30, 3021–3033. (in Chinese with English abstract)
- Yang, J., Gao, S., Hu, Z., Yuan, H., Gong, H., Li, M., Xiao, G., and Wei, J., 2008, Age and growth of the Archean Kongling terrain, South China, with emphasis on 3.3 Ga granitoid gneisses. *Geochimica et Cosmochimica Acta*, 72, 153–182.

- Zhang, S.B., Zheng, Y.F., Wu, Y.B., and Wu, F.Y., 2006a, Zircon U-Pb age and Hf-O isotope evidence for Paleoproterozoic metamorphic event in South China. *Precambrian Research*, 151, 265–288.
- Zhang, D.L., Huang, D.Z., Zhang, H.F., Wang, G.Q., and Du, G.F., 2016, Chronological framework of basement beneath the Xiangmgzhong Basin: evidence by U-Pb ages of detrital zircons from Xikuangshan. *Acta Petrologica Sinica*, 32, 3456–3468. (in Chinese with English abstract)
- Zhang, L.J., Ma, C.Q., Wang, L.X., She, Z.B., and Wang, S.M., 2011, Discovery of Paleoproterozoic rapakivi granite on the northern margin of the Yangtze block and its geological significance. *Chinese Science Bulletin*, 56, 306–318.
- Zhang, S.B., Zheng, Y.F., Wu, Y.B., Zhao, Z.F., Gao, S., and Wu, F.Y., 2006b, Zircon isotope evidence for  $\geq 3.5$  Ga continental crust in the Yangtze craton of China. *Precambrian Research*, 146, 16–34.
- Zhao, G., Cawood, P.A., Wilde, S.A., and Sun, M., 2002, Review of global 2.1–1.8 Ga orogens: implications for a pre-Rodinia supercontinent. *Earth-Science Reviews*, 59, 125–162.
- Zhao, G.C., Li, S.Z., Sun, M., and Wilde, S.A., 2011, Assembly, accretion, and break-up of the Paleo-Mesoproterozoic Columbia supercontinent: record in the North China Craton revisited. *International Geology Review*, 53, 1331–1356.
- Zhao, G.C., Sun, M., Wilde, S.A., and Li, S.Z., 2004, A Paleo-Mesoproterozoic Supercontinent: assembly, growth and breakup. *Earth-Science Reviews*, 67, 91–123.
- Zhao, X.F., Zhou, M.F., Li, J.W., Sun, M., Gao, J.F., Sun, W.H., and Yang, J.H., 2010, Late Paleoproterozoic to early Mesoproterozoic Dongchuan Group in Yunnan, SW China: implications for tectonic evolution of the Yangtze Block. *Precambrian Research*, 182, 57–69.
- Zheng, J., Griffin, W.L., O'Reilly, S.Y., Zhang, M., Pearson, N., and Pan, Y.M., 2006, Widespread Archean basement beneath the Yangtze craton. *Geology*, 34, 417–420.
- Zhou, M.F., Arndt, N.T., Malpas, J., Wang, C.Y., and Kennedy, A., 2008, Two magma series and associated ore deposit types in the Permian Emeishan large igneous province, SW China. *Lithos*, 103, 352–368.
- Zhou, M.F., Zhao, X.F., Chen, W.T., Li X.C., Wang, W., Yan, D.P., and Qiu, H.N., 2014, Proterozoic Fe-Cu metallogeny and supercontinental cycles of the southwestern Yangtze Block, southern China and northern Vietnam. *Earth-Science Reviews*, 139, 59–82.

**Publisher's Note** Springer Nature remains neutral with regard to jurisdictional claims in published maps and institutional affiliations.